# $Ca^{2+}$ signaling evoked by activation of $Na^+$ channels and $Na^+/Ca^{2+}$ exchangers is required for GABA-induced NG2 cell migration

Xiao-ping Tong, Xiang-yao Li, Bing Zhou, Wanhua Shen, Zhi-jun Zhang, Tian-le Xu, Shumin Duan

Institute of Neuroscience and State Key Laboratory of Neuroscience, Shanghai Institutes for Biological Sciences, Chinese Academy of Sciences, Shanghai 200031, China

NG2 cells originate from various brain regions and migrate to their destinations during early development. These cells express voltage-gated $Na^+$ channels but fail to produce typical action potentials. The physiological role of $Na^+$ channels in these cells is unclear. We found that GABA induces membrane depolarization and $Ca^{2+}$ elevation in NG2 cells, a process requiring activation of $GABA_A$ receptors, $Na^+$ channels, and $Na^+/Ca^{2+}$ exchangers (NCXs), but not $Ca^{2+}$ channels. We have identified a persistent $Na^+$ current in these cells that may underlie the GABA-induced pathway of prolonged $Na^+$ elevation, which in turn triggers $Ca^{2+}$ influx via NCXs. This unique $Ca^{2+}$ signaling pathway is further shown to be involved in the migration of NG2 cells. Thus, GABAergic signaling mediated by sequential activation of $GABA_A$ receptors, noninactivating $Na^+$ channels, and NCXs may play an important role in the development and function of NG2 glial cells in the brain.

## Introduction

NG2 cells are characterized by expression of the chondroitin sulfate proteoglycan NG2 and have been described under different terms including oligodendrocyte progenitor cells (OPCs) that generate oligodendrocytes in the developing brain. NG2 cells are also abundant in the mature central nervous system (CNS). Morphologically, OPCs typically have bipolar processes, whereas NG2 cells in adult brain have multiple branched processes. These cells in both developing and adult brain share a similar phenotype by expressing PDGFα receptors (Nishiyama et al., 1996; Stallcup, 2002). Although the exact functions of NG2 cells in adult brain are not clear, these cells are thought to divide and regenerate oligodendrocytes in response to demyelination caused by various neural injury.

NG2 cells exhibit electrophysiological properties distinct from neurons and other types of glial cells. Although NG2 cells have a membrane potential close to the $K^+$ equilibrium potential, they have a high membrane resistance and do not exhibit dye coupling through gap junctions (Butt et al., 2002; Chittajallu et al., 2004; Paukert and Bergles, 2006). Application of depolarizing voltage steps activates multiple types of voltage-gated channels, including tetrodotoxin (TTX)-sensitive $Na^+$ channels. Unlike that found in neurons, however, activation of $Na^+$ channels in NG2 cells only induces small transient depolarization, without firing of typical action potentials (Barres et al., 1990; Bergles et al., 2000; Lin and Bergles, 2004b; Ge et al., 2006; see Káradóttir et al., 2008). Thus, the functional role of the $Na^+$ channels in NG2 cells has been unclear.

Another interesting property of NG2 cells is that they receive direct glutamatergic and GABAergic synaptic inputs from neurons (Bergles et al., 2000; Lin and Bergles, 2004a). They express $Ca^{2+}$-permeable AMPA receptors that may mediate $Ca^{2+}$ influx and trigger important cellular processes, including the induction of long-term potentiation (Ge et al., 2006). The functional role of GABAergic activation of NG2 cells, however, remains unclear. Activation of $GABA_A$ receptor ($GABA_AR$) on neurons is known to induce either depolarization or hyperpolarization, depending on $[Cl^-]_i$, which is in turn regulated by the $Na^+$-$K^+$-$Cl^-$ cotransporter 1 (NKCC1) and $K^+$-$Cl^-$ cotransporter 2 (KCC2) that transport $Cl^-$ into and out of the cell, respectively. Immature neurons maintain a high

Correspondence to Shumin Duan: shumin@ion.ac.cn

Abbreviations used in this paper: ACSF, artificial cerebrospinal fluid; CNS, central nervous system; DiI, 1,1′-dioctadecyl-3,3,3′,3′ tetramethylindocarbocyanine; ECS, extracellular solution; $GABA_AR$, $GABA_A$ receptor; GDP, giant depolarizing potential; GFAP, glial fibrillary acidic protein; NCX, $Na^+/Ca^{2+}$ exchanger; NKCC1, $Na^+$-$K^+$-Cl− cotransporter 1; OPC, oligodendrocyte progenitor cell; SBFI/AM, sodium-binding benzofuran isophthalate; SVZ, subventricular zone; TTX, tetrodotoxin; VGCC, voltage-gated $Ca^{2+}$ channel.



The Rockefeller University Press $30.00
J. Cell Biol. Vol. 186 No. 1 113–128
www.jcb.org/cgi/doi/10.1083/jcb.200811071

$[Cl^-]_i$ because of their high expression level of NKCC1, low level of KCC2, and response to GABA with depolarization, which may exert excitatory effects by the activation of voltage-dependent $Na^+$ channels to trigger action potentials, the activation of voltage-dependent $Ca^{2+}$ channels to elevate $[Ca^{2+}]_i$, and the removal of $Mg^{2+}$ blockade of NMDA receptors to enhance $Ca^{2+}$ influx through NMDA receptors (Ben-Ari, 2002; Owens and Kriegstein, 2002; Ben-Ari et al., 2007). Activation of $GABA_A$Rs in hippocampal NG2 cells has been reported to induce membrane depolarization and inhibit AMPA receptor–mediated currents (Lin and Bergles, 2004a). However, NG2 cells do not express voltage-activated $Ca^{2+}$ channels (Sontheimer et al., 1989; Ge et al., 2006). Although some subpopulation of NG2 cells in the cerebellar white matter may express NMDA receptors (Káradóttir et al., 2005; Ziskin et al., 2007) or fire action potentials (Káradóttir et al., 2008), most NG2 cells in the brain do not fire action potentials (Barres et al., 1990; Bergles et al., 2000; Lin and Bergles, 2004b; Ge et al., 2006), nor do they express NMDA receptors in the hippocampus (Ge et al., 2006). The functional consequence of this depolarization remains to be determined.

During development, NG2 cells are generated in the ventricular zone and migrate over long distances to their destinations (Small et al., 1987; Cameron-Curry and Le Douarin, 1995; Spassky et al., 1998; Menn et al., 2006). Directed migration of these glial progenitor cells is essential not only for myelin formation in the developing brain but also for myelin repair after injury (Blakemore and Keirstead, 1999; Keirstead et al., 1999; Chang et al., 2000; Franklin, 2002; Zhang et al., 2004; Aguirre et al., 2007). However, unlike the case of neuronal migration, the guidance cues and cellular signaling mechanisms of glial cell migration are much less understood. Activation of $GABA_A$Rs in immature neurons or neuronal progenitor cells is involved in neural development, including neurogenesis, neuronal differentiation, and neuronal migration, an effect involving $Ca^{2+}$ influx through voltage-gated $Ca^{2+}$ channels (VGCCs) activated by GABA-induced membrane depolarization (Behar et al., 1996, 1998; Maric et al., 2001; Owens and Kriegstein, 2002; Nguyen et al., 2003; Marty and Llano, 2005; Akerman and Cline, 2007; Ben-Ari et al., 2007; Bordey, 2007; Heng et al., 2007). In the present study, we found that GABA-induced membrane depolarization in NG2 cells activates a persistent $Na^+$ current, which in turn induces $[Ca^{2+}]_i$ elevation via the reversed activity of type I $Na^+/Ca^{2+}$ exchangers (NCX1). Further evidence indicates that this unique pathway is involved in the NG2 cell migration.

## Results

### Depolarization-induced persistent $Na^+$ currents in NG2 cells

Whole-cell recordings were made from NG2 cells in the CA1 region of hippocampal slices from postnatal d 7–17 (P7–P17) rats. NG2 cells were identified by having a high input resistance, transient A-type and delayed-rectifier $K^+$ currents, and small TTX–sensitive $Na^+$ currents that fail to generate typical action potentials (Fig. 1 A, see Bergles et al., 2000; Ge et al., 2006). The kinetics

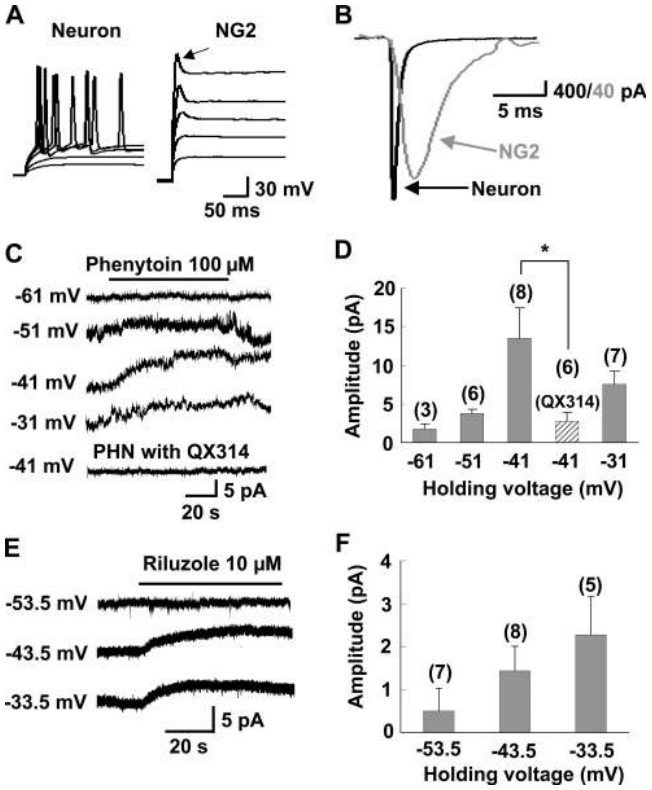


Figure 1. **Persistent $Na^+$ currents recorded from NG2 cells in hippocampal slices.** (A) Superimposed membrane potential changes in an NG2 cell and a pyramidal neuron in response to a series of current injections (300 ms in duration with an interval of 15 s) from a holding potential of −70 and −60 mV, respectively. In the NG2 cell, only a single small spikelike depolarizing transient (arrow) could be evoked upon each super-threshold depolarizing current injection. (B) Comparison of the kinetics of $Na^+$ currents recorded from a NG2 cell with those recorded from a neuron evoked by a depolarizing voltage pulse at –20 mV. (C) Example recordings from NG2 cells showing phenytoin-induced persistent outward current at −41 or −31 mV holding membrane potential and its blockage by intracellular loading QX314 (5 mM; bottom trace). (D) Mean amplitude of phenytoin-induced outward currents recorded at various membrane potentials as shown in C. The number associated with each column refers to the number of cells examined in each condition. *, $P < 0.05$ compared with the group as indicated. (E) Perfusion with riluzole also revealed an apparent persistent outward current at depolarizing membrane potentials. (F) Mean amplitude of riluzole-induced outward currents recorded at various membrane potentials as shown in E. Error bars represent mean ± SEM.

of this transient $Na^+$ current were significantly slower than those found in neurons (Fig. 1 B). We found that, when a recording was made at membrane potentials more positive than −40 mV, bath-application of phenytoin or riluzole, antagonists of persistent component of $Na^+$ channels (Kononenko et al., 2004; Ptak et al., 2005; Zeng et al., 2005), induced a sustained outward current in the NG2 cell (Fig. 1, C–F), which is consistent with the removal of a noninactivating $Na^+$ conductance (Stys et al., 1993; Kononenko et al., 2004; Ptak et al., 2005). Furthermore, when the recording pipette contained *N*-(2,6-dimethylphenylcarb amoylmethyl)triethylammonium bromide (QX314), an intracellular sodium channel blocker, phenytoin-induced outward currents were absent (Fig. 1, C and D), which confirms the notion that phenytoin-induced outward currents were caused by the blockade of persistent $Na^+$ currents.

### $GABA_AR$ activation induces membrane depolarization

Whole cell recordings were made from an NG2 cell in hippocampal slices from P7–P10 rats. We found that perfusion of NG2 cells with 100 μM GABA or 50 μM of the selective $GABA_AR$ agonist muscimol induced a substantial inward current (GABA: −168 ± 96 pA, $n = 5$; muscimol: −186 ± 70 pA, $n = 5$). Gramicidin-perforated patch recording showed that 50 μM muscimol induced a significant depolarization of NG2 cells (16.1 ± 2.5 mV, $n = 7$) at a holding membrane potential of −70 mV, and application of 10 μM of NKCC1 inhibitor bumetanide reduced the muscimol responses to 9.2 ± 2.6 mV ($n = 7$; Fig. 2 B). In addition, we found that perfusion of the $GABA_AR$ antagonist bicuculline induced membrane hyperpolarizations (−5.6 ± 1.1 mV, $n = 11$) or outward currents (26.7 ± 6.1 pA, $n = 8$) in NG2 cells (Fig. 2 C), which is consistent with the presence of tonic GABA release in the early developmental brain and adult subventricular zone (SVZ; Cherubini et al., 1991; Brickley et al., 1996; Semyanov et al., 2004; Bordey, 2007). Furthermore, bicuculline-sensitive spontaneous transient inward currents were also recorded in some NG2 cells (two out of eight cells examined; Fig. 2 C), which indicates that activity-evoked phasic GABA release could be detected by NG2 cells.

The reversal potential of muscimol-induced depolarization was found to be −33.6 ± 4.3 mV ($n = 4$), corresponding to 35.2 mM $[Cl^-]_i$, based on the Nernst equation and corrected for $HCO_3^-$ contribution (Lin and Bergles, 2004a; Kim and Trussell, 2007). When slices were pretreated with bumetanide (10 μM, 5 min), the reversal potential was shifted toward a more negative potential (−44.2 ± 7.0 mV, $n = 4$; Fig. 2, D–F), which indicates that, similar to case of immature neurons (Yamada et al., 2004; Brumback and Staley, 2008), NKCC1 transporter activity was responsible for the high $[Cl^-]_i$ in these NG2 cells. It should be noted that in the presence of the bumetanide, the GABA-induced current was still reversed at a relatively depolarizing level as compared with the resting membrane potential, which suggests that, in addition to NKCC1, NG2 cells may also express other unknown types of inward $Cl^-$ transporters. We found that 50 μM muscimol still induced depolarizing responses (15.7 ± 2.4 mV, $n = 6$) in NG2 cells in adult hippocampal slices (P28–P32) when recorded at a membrane potential of −70 mV using gramicidin-perforated patch recordings, which indicates that, unlike neurons, NG2 cells lack apparent developmental switch for the GABA-induced responses.

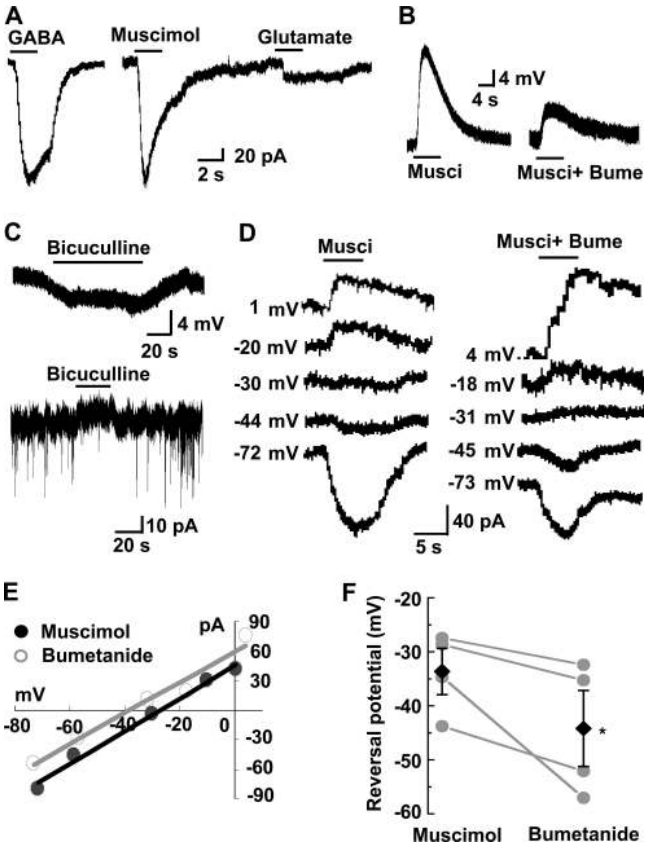


Figure 2. **$GABA_AR$-mediated responses in NG2 cells in hippocampal slices under gramicidin-perforated patch recording.** (A) Comparing the 100 μM GABA-, 50 μM muscimol-, and 100 μM glutamate-induced currents in a single NG2 cell. (B) 50 μM muscimol-induced depolarization and its inhibition by treatment with 10 μM bumetanide. (C, top) Perfusion with 10 μM bicuculline induced a membrane hyperpolarization in an NG2 cell, which indicates a persistent membrane depolarization induced by the tonic released GABA. (C, bottom) An example of a voltage-clamp recording from an NG2 cell showing that bicuculline not only induced a persistent outward current, but also blocked the spontaneous transient inward currents, demonstrating the tonic and phasic GABA release sensed by the NG2 cell in the brain slice. (D) The 50 μM muscimol-evoked currents in a single NG2 cell were estimated at various membrane potential levels in the presence and absence of 10 μM bumetanide. The number at the left of each trace indicates membrane potential (Vm) after correction for access resistance (see Materials and methods). (E) Current-voltage (I-V) plots of the muscimol-evoked currents shown in D. Regression lines were made based on the plotted data. (F) Summary of the reversal potentials of the muscimol-evoked currents determined by the intersection of the regression lines at the x axis of I-V plots shown in E. Each line connects the data collected from the same cell in the absence (left) and presence (right) of 10 μM bumetanide. Black diamonds represent mean reversal potentials in each group. *, $P < 0.05$ compared with the muscimol group. Error bars represent mean ± SEM.

### $GABA_AR$ activation induces $[Ca^{2+}]_i$ elevation

To directly examine the functional role of $GABA_AR$ activation in NG2 cells, we loaded hippocampal slices with the fluorescent $Ca^{2+}$ indicator Fluo-4 AM and monitored the changes of $[Ca^{2+}]_i$. Using an antibody that recognizes the extracellular domain of NG2, we labeled living NG2 cells by surface immunostaining (Fig. 3, A and B; Káradóttir et al., 2008). We found that perfusion with GABA induced a significant $[Ca^{2+}]_i$ elevation in NG2-positive cells, an effect that was abolished by coperfusion with bicuculline but unaffected by the $GABA_B$ antagonist (2S)-3-[[(1S)-1-(3,4-dichlorophenyl)ethyl]amino-2-hydroxypropyl](phenylmethyl)phosphinic acid (CGP 55845) or the general $Ca^{2+}$ channel antagonist $Cd^{2+}$ (Fig. 3, B–D and Video 1).

### GABA-induced $[Ca^{2+}]_i$ elevation requires activation of $Na^+$ channels and NCXs

NCX is known to regulate $[Ca^{2+}]_i$, although in neurons, the $Ca^{2+}$ entry mediated by NCX is minor compared with that entry through VGCCs (Annunziato et al., 2004). Because muscimol induced substantial membrane depolarizations (Fig. 2 B), and the persistent $Na^+$ conductance was activated at a relatively negative membrane potential (−50 mV) in NG2 cells (Fig. 1, C–F),

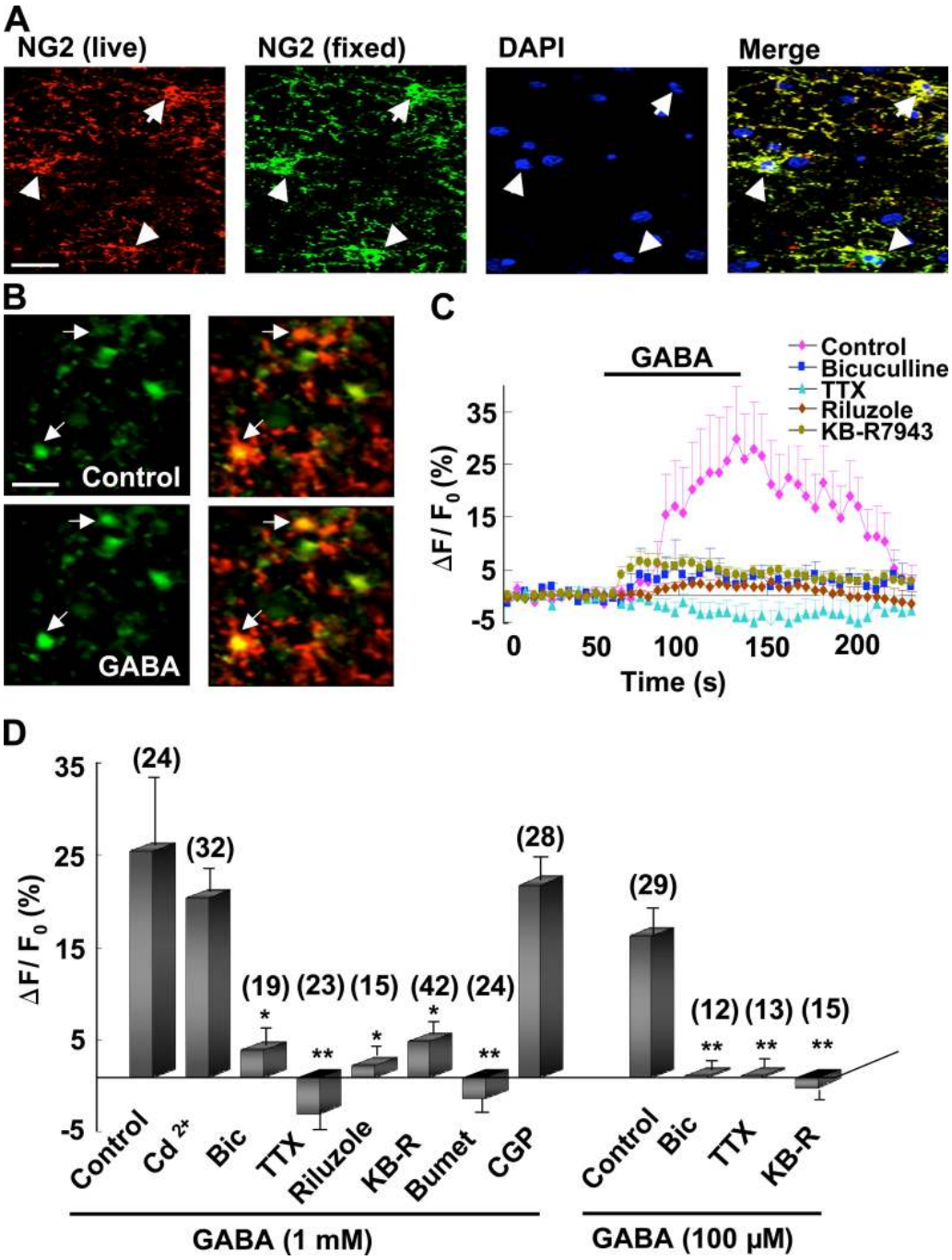


Figure 3. **GABA-induced $[Ca^{2+}]_i$ elevation in NG2 cells in hippocampal slices.** (A) The slice was live stained with NG2 (red, anti–mouse) and then fixed by 4% paraformaldehyde for the secondary anti-NG2 immunostaining (green, anti–rabbit). The two sets of staining colocalized nicely, which excluded the possibility of nonspecific staining of live cells due to endocytosis of the antibody. The nucleus was stained by DAPI (blue). Typical NG2 cells are indicated by white arrows and arrowheads. Bar, 20 μm. (B) Confocal images of NG2 cells loaded with Fluo-4 AM (green). The NG2 cells were identified by live immunostaining with anti-NG2 (red). Note the increased $[Ca^{2+}]_i$ in NG2 cells (indicated by arrows) during 1 mM GABA perfusion. 500 μM kynurenic acid was added to block potential secondary activation of glutamate receptors. Bar, 20 μm. (C) Time course of GABA-induced $[Ca^{2+}]_i$ changes in NG2 cells with or without the presence of various inhibitors. (D) Summary of GABA-induced $[Ca^{2+}]_i$ changes in NG2 cells as shown in C. Data were averaged during 55–105 s after the onset of perfusion with GABA, and normalized by the mean fluorescence intensity obtained during the control period (0–50 s before GABA perfusion) for each cell. *, $P < 0.05$; **, $P < 0.01$ compared with the corresponding control group. Error bars represent mean ± SEM.

we examined the possibility that GABA-induced depolarization may activate the persistent $Na^+$ conductance, allowing $Na^+$ influx, which in turn triggers $Ca^{2+}$ influx through the reversed NCX activity. Consistent with this hypothesis, we found that GABA failed to induce $[Ca^{2+}]_i$ elevation in NG2 cells when the hippocampal slice was coperfused with TTX or riluzole. Furthermore, a blockade of NCX activity with the specific NCX antagonist 2-[2-[4-(4-nitrobenzyloxy)phenyl]ethyl]isothiourea mesylate (KB-R7943; Annunziato et al., 2004) abolished GABA-induced $[Ca^{2+}]_i$ elevation (Fig. 3, C and D). Interestingly, treatment

of the slices with bumetanide also abolished the GABA-induced $[Ca^{2+}]_i$ elevation, which suggests that NKCC1 activity sets the reversal potential of $GABA_AR$-mediated current to a critical level for the activation of $Na^+$ channels and the subsequent influx of $Ca^{2+}$ through NCX.

### GABA induces $[Ca^{2+}]_i$ elevation in acutely dissociated NG2 cells

To further study the mechanisms of GABA-induced $[Ca^{2+}]_i$ in NG2 cells and to exclude the possibility that GABA-induced $[Ca^{2+}]_i$ elevation in NG2 cells in the slice preparation might be caused by GABA-induced release of some unknown factors from other cell types in the brain, we have examined whether GABA affected $[Ca^{2+}]_i$ in acutely dissociated NG2 cells. Acutely dissociated NG2 cells from hippocampal slices were identified by live surface immunostaining with anti-NG2 antibody. As shown in Fig. 4 (A–C), the dissociated NG2-positive cells responded to GABA with an increased $[Ca^{2+}]_i$, which was blocked by coperfusion with bicuculline, TTX, or KB-R7943, but not with the L-type $Ca^{2+}$ channel blocker nimodipine.

### GABA-induced $[Ca^{2+}]_i$ signaling in cultured NG2 cells

Purified NG2 cultures contained cells that showed the typical morphology of NG2 cells, with >95% of them stained positive for NG2 (Fig. 5 A and Fig. S1 A). The antigen phenotype of the cultured cells was further confirmed by double immunostaining of anti-NG2 and antibodies for various neuronal and glial markers. As shown in Fig. S1 B, the NG2-positive cells are also immunopositive for $PDGF_\alpha$ receptors, another characteristic marker of NG2 cells, but are negative for the markers of the neuron (βIII tubulin), astrocyte (glial fibrillary acidic protein [GFAP]), or microglia (CD11b), which is consistent with previous findings (Nishiyama et al., 1996, 2002; Levine et al., 2001; Butt et al., 2002).

Whole-cell recordings showed that these cultured cells had similar electrophysiological properties to those recorded from NG2 cells in brain slices (Ge et al., 2006; Paukert and Bergles, 2006), including high input resistance (1.67 ± 0.21 GΩ, $n$ = 37 cells), negative resting membrane potential (−76.7 ± 5.0 mV, $n$ = 21 cells), and TTX-sensitive transient inward currents or depolarizations (Fig. 5, B and C). No detectable VGCCs were recorded in these cultured cells (Fig. 5 D), which is consistent with findings in NG2 cells in brain slices (Ge et al., 2006). We found that TTX induced a significant sustained outward current in cultured NG2 cells when recorded at a membrane potential more positive than −40 mV (Fig. 5, E and F), which confirmed the presence of noninactivating $Na^+$ channels. The small persistent $Na^+$ current induced by depolarizing pulses (Fig. 5 C) may be masked by the residual outward $K^+$ currents or leak currents, even in the presence of $K^+$ channel blockers. We further showed that perfusion of GABA induced apparent bicuculline-sensitive inward current in cultured NG2 cells under the whole-cell recording with high $Cl^-$ concentration in the recording pipettes (Fig. 5 G). Further gramicidin-perforated recording showed that 1 mM GABA induced 28.0 ± 3.9 mV ($n$ = 7 cells) depolarization from a resting membrane potential

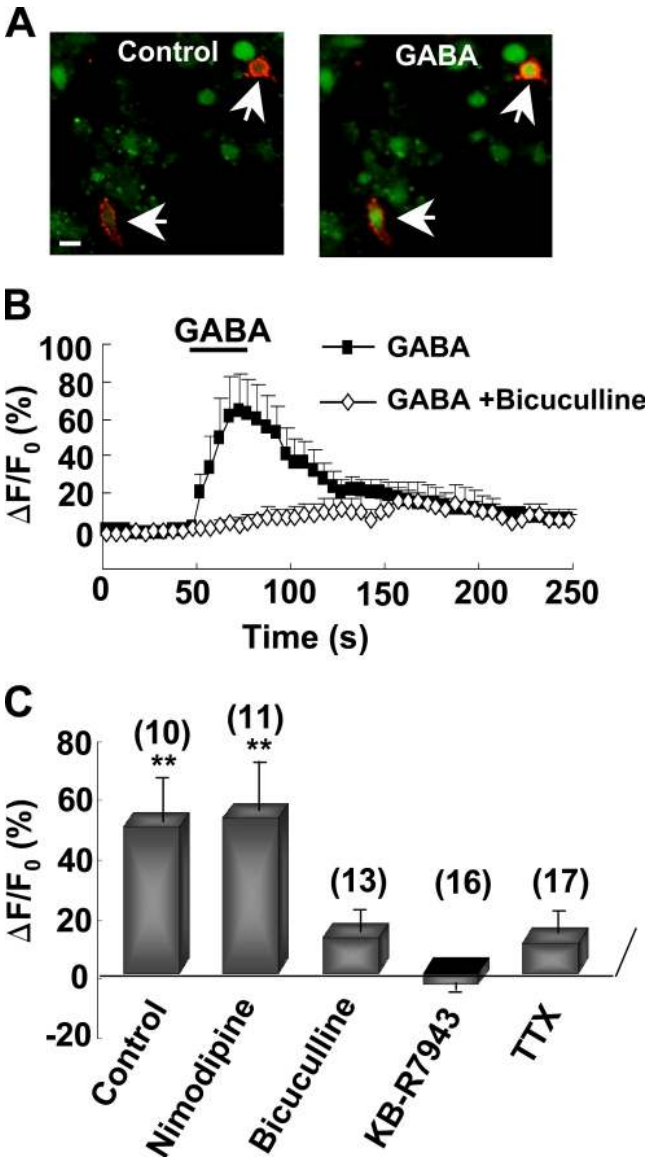


Figure 4. **GABA-induced $[Ca^{2+}]_i$ elevation in acutely dissociated NG2 cells.** (A) Images of acutely dissociated NG2 cells (arrows) loaded with the Fluo4-AM (green) and identified by live immunostaining with anti-NG2 (red). Images were taken from the same imaging field before (control) and during perfusion with 1 mM GABA. Bar, 10 µm. (B) Time course of $[Ca^{2+}]_i$ changes in dissociated NG2 cells perfusion with 1 mM GABA with or without 10 µM bicuculline. (C) Summary of GABA-induced $[Ca^{2+}]_i$ changes in dissociated NG2 cells with or without various inhibitors. Data were averaged during 20–50 s after the onset of perfusion with GABA, and normalized by the mean fluorescence intensity obtained during the control period (0–50 s before GABA perfusion) for each cell. **, P < 0.01 compared with ECS group not treated with GABA. Error bars represent mean ± SEM.

of −70 mV (Fig. 5 H). Together, these results indicate that cultured NG2 cells have similar electrophysiological properties to those found for NG2 cells in brain slices.

We found that GABA induced a bicuculline-sensitive $[Ca^{2+}]_i$ elevation in cultured NG2 cells (Fig. 6, A–C and Video 2). This $[Ca^{2+}]_i$ elevation depended on the presence of $Ca^{2+}$ in the extracellular solution (ECS), but nifedipine had no effect on this $[Ca^{2+}]_i$ increase (Fig. 6 C), which is consistent with the lack of L-type VGCCs in these cells (Fig. 5 D). Furthermore,

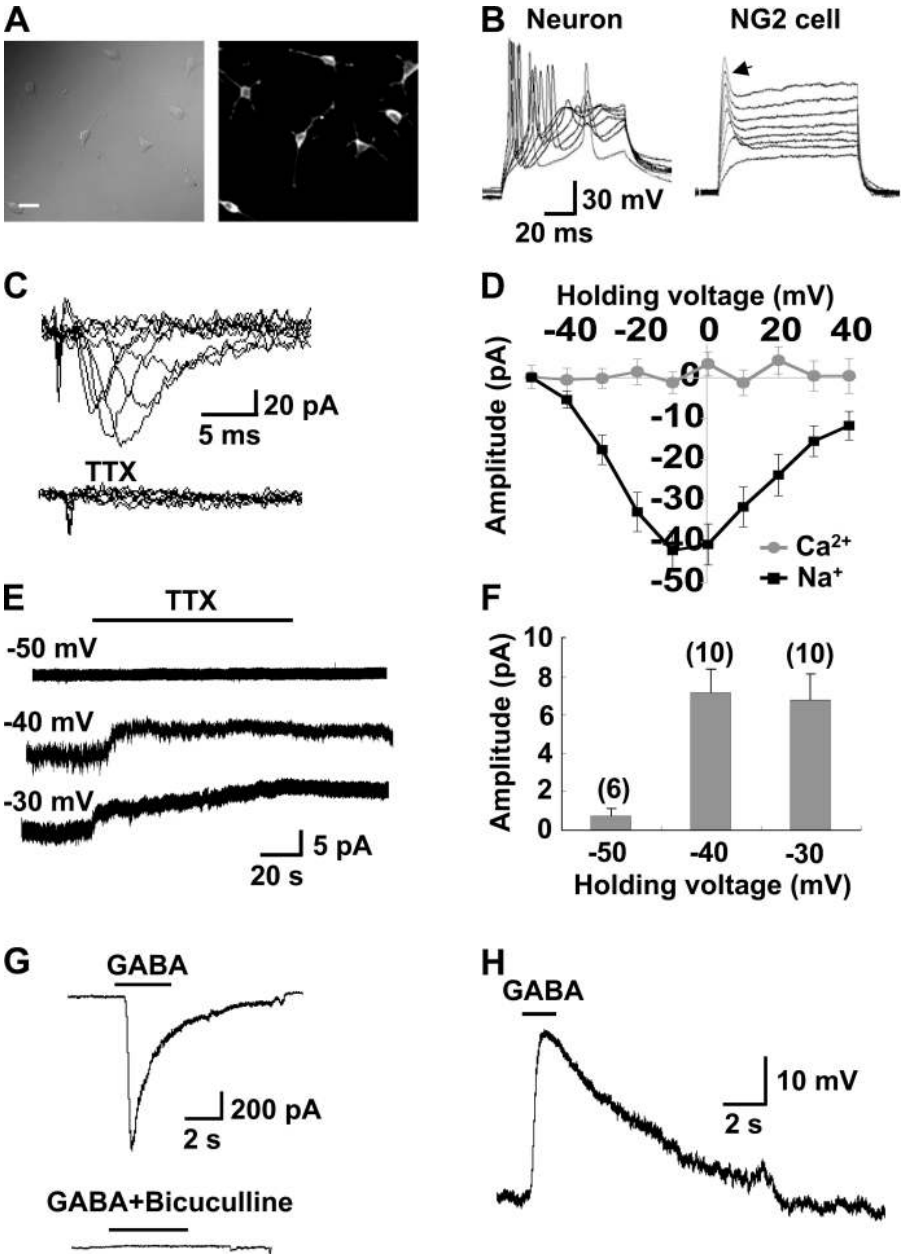


Figure 5. **Electrophysiological properties of cultured NG2 cells.** (A) Phase contrast (left) and fluorescence (right) images of purified NG2 cells immunostained with anti-NG2 antibody. Bar, 20 µm. (B) Comparison of the properties of membrane potential changes in a cultured NG2 cell and a neuron in response to a series of depolarizing current injections with an increment of 50 pA at an interval of 10 s at a −70 mV holding potential. Note the increased amplitude of the initial transient depolarizations (arrow) in the NG2 cell. (C) TTX-sensitive transient $Na^+$ currents (top traces) recorded from a cultured NG2 cell evoked by voltage steps (100 ms, 10 mV increment) from –60 to +50 mV, with a 300-ms prepulse of −110 mV. (D) I-V plots of $Na^+$ and $Ca^{2+}$ currents in cultured NG2 cells evoked by depolarizing voltage steps as shown in C. Note the lack of apparent voltage-gated $Ca^{2+}$ currents in NG2 cells. (E) Recording traces from a cultured NG2 cell showing that perfusion with 0.5 µM TTX revealed a persistent outward current at −40 or −30 mV, but not at a −50 mV holding membrane potential. (F) Mean amplitude of TTX-induced outward currents recorded under various membrane potentials as shown in E. Error bars represent mean ± SEM. (G) Whole-cell recording from a cultured NG2 cell showing 50 µM GABA–induced inward current and its blockade by 10 µM bicuculline at −70 mV membrane potential. (H) 1 mM GABA–induced depolarization in an NG2 cell under gramicidin-perforated recording at −70 mV membrane potential.

GABA failed to induce $[Ca^{2+}]_i$ elevation when these cells were perfused with $Na^+$-free or TTX-containing solution, or with KB-R7943 (Fig. 6 C).

### Down-regulation of NCX1 or $Na^+$ channels by siRNA prevents GABA-induced $[Ca^{2+}]_i$ signaling

Three subtypes of NCX are expressed in the brain (Blaustein and Lederer, 1999; Thurneysen et al., 2002; Annunziato et al., 2004). Using commercially available antibodies specific for NCX1 and NCX2 subtypes, respectively, we found that although neurons intensively express both NCX1 and NCX2, NG2 cells express intensive NCX1 but very weak NCX2, as examined by immunostaining in either cortical slices (Fig. S2) or purified NG2 cultures (Fig. S3). We thus down-regulated expression of NCX1 in cultured NG2 cells using siRNA, an efficient approach used extensively to knock down specific gene expression in cells. We used an siRNA sequence specifically targeted to NCX1 (siNCX1), the efficiency of which has been verified previously (Slodzinski and Blaustein, 1998). We found that the fluorescence signal of anti-NCX1 in NG2 cells transfected with siNCX1 was reduced to a level ∼38% of untransfected cells. Transfection with scrambled siRNA did not affect expression of NCX1 in NG2 cells (Fig. S4, A and C). GABA-induced $Ca^{2+}$ signaling was largely inhibited in cells transfected with siNCX1, but not in cells transfected with scrambled siRNA (Fig. 6, D and E). Thus, NCX1 is the major subtype of NCX mediating GABA-induced $Ca^{2+}$ signaling in NG2 cells.

To further confirm the involvement of $Na^+$ channels in the GABA-induced signaling in NG2 cells, we reduced expression of $Na^+$ channels using siRNA-Nav1.x (siNav1.x) targeting to multiple subtypes of rat $Na^+$ channels. Immunostaining with

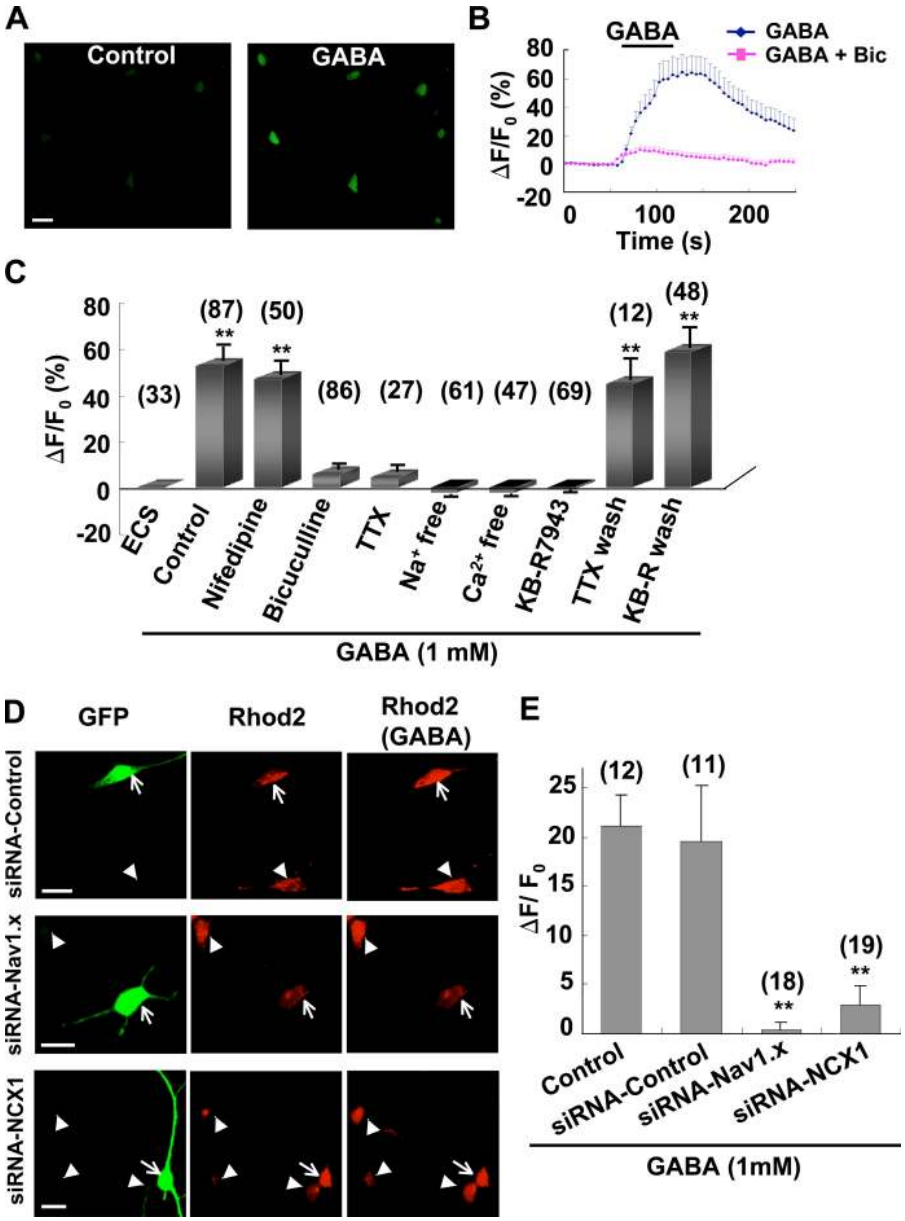


Figure 6. **GABA-induced $[Ca^{2+}]_i$ elevation in cultured NG2 cells.** (A) Confocal images of cultured NG2 cells loaded with Fluo-4 AM before (control) and during perfusion with 1 mM GABA. Bar, 20 µm. (B) Averaged time course of 1 mM GABA–induced $[Ca^{2+}]_i$ elevation in cultured NG2 cells and its blockage by 10 µM bicuculline. (C) Summary of $[Ca^{2+}]_i$ changes in NG2 cells perfused with normal solution (ECS) or solution containing 1 mM GABA with or without (control) various treatments. Data are averaged during 30–80 s after the onset of perfusion with GABA, normalized by the mean fluorescence intensity obtained during the control period (0–50 s before GABA perfusion) for each cell. TTX wash and KB-R wash, recovery of the GABA-induced $[Ca^{2+}]_i$ elevation after 10 min and 5 min wash out of 1 µM TTX and 10 µM KB-R7943, respectively. **, $P < 0.01$ compared with ECS group. (D, left) Confocal images of cultured NG2 cells cotransfected with pGFP + scrambled siRNA (siRNA-Control), pGFP + siRNA-Nav1.x, or pGFP+siRNA-NCX1, respectively. (D, middle and right) $[Ca^{2+}]_i$ images of untransfected (arrowheads) and transfected (arrows) NG2 cells loaded with the $Ca^{2+}$ dye Rhod2 AM before and during perfusion with 1 mM GABA, respectively. Images in each row were sampled from the same field. Note that GABA induced apparent $[Ca^{2+}]_i$ elevation in untransfected cells or cells transfected with siRNA-control, but not in cells transfected with either siRNA-Nav1.x or siRNA-NCX1. Bars, 20 µm. (E) Summary of GABA-induced $[Ca^{2+}]_i$ changes in NG2 cells with or without various transfections. Data are averaged during 30–100 s after the onset of perfusion with GABA, subtracted by the mean fluorescence intensity obtained during the control period (0–50 s before GABA perfusion) for each cell. **, $P < 0.01$ compared with siRNA control group. Error bars represent mean ± SEM.

anti-pan-Nav, which labels all isoforms of Nav, showed a significant decreased expression of $Na^+$ channels in cells transfected with siNav1.x, as compared with untransfected cells or cells transfected with scrambled siRNA (Fig. S4, B and C), confirming the efficiency of the siNav1.x described previously (Xu and Shrager, 2005). Moreover, $Na^+$ currents recorded in NG2 cells transfected with siNav1.x were largely blocked (Fig. S4, D and E). Furthermore, we found that GABA-induced $[Ca^{2+}]_i$ elevation was blocked in cells transfected with siNav1.x but not in cells transfected with scrambled siRNA (Fig. 6, D and E).

Collectively, by using various chemical inhibitors for functional blockage and an siRNA approach for specific down-regulation of protein expression in purified NG2 cultures that are relatively free of secondary effects from other cell types, we confirmed our findings in hippocampal slices and further supported the notion that activation of $GABA_A$Rs in NG2 cells results in membrane depolarization and activation of noninactivating $Na^+$ channels, which in turn allows the persistent $Na^+$ influx that triggers the reversed NCX activity, leading to $[Ca^{2+}]_i$ elevation.

### GABA-induced $Na^+$ influx in cultured NG2 cells

To detect $[Na^+]_i$ changes directly, we performed $Na^+$ imaging with sodium-binding benzofuran isophthalate (SBFI/AM; Rose et al., 1998). We found that perfusion with GABA induced a sustained increase in $[Na^+]_i$ in cultured NG2 cells. The GABA-induced $[Na^+]_i$ increase was blocked by bicuculline or TTX (Fig. 7, A–C), which is consistent with $Na^+$ influx via $Na^+$ channels activated by $GABA_A$R-mediated depolarization. Similarly, perfusion with muscimol also induced $[Na^+]_i$ elevation, an effect that was abolished by coperfusion with TTX or bicuculline (Fig. 7 C). However, perfusion with the NCX inhibitor KB-R7943 enhanced muscimol-induced $[Na^+]_i$ elevation (Fig. 7 C),

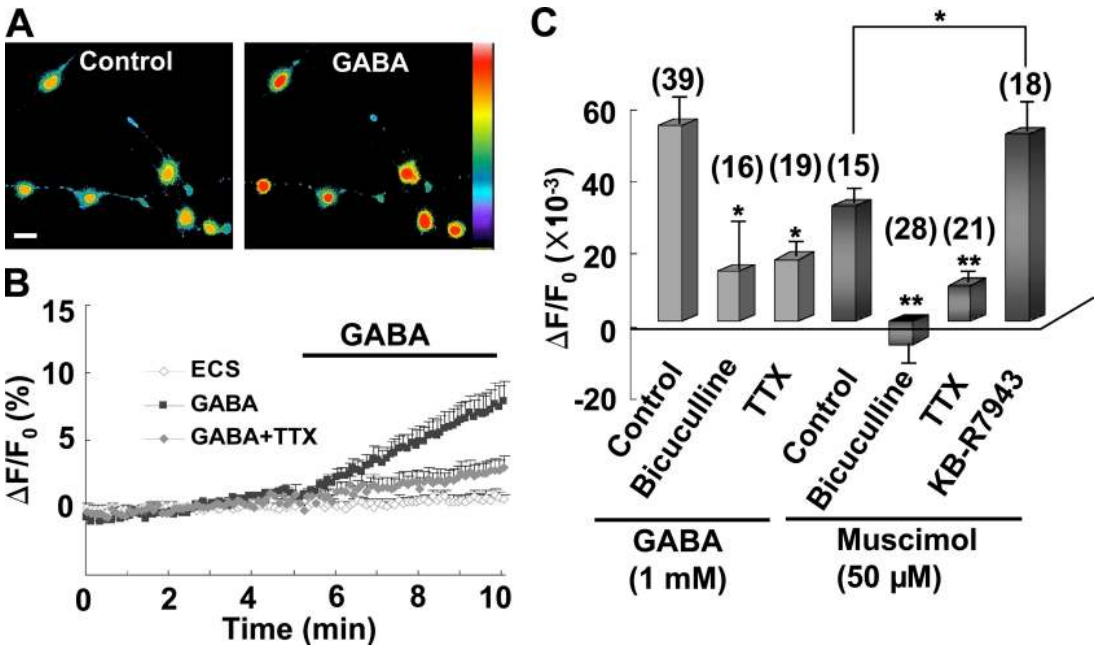


Figure 7. **GABA-induced $[Na^+]_i$ elevation in cultured NG2 cells.** (A) Confocal images of cultured NG2 cells preloaded with the $Na^+$ dye SBFI/AM. Images were taken from the same imaging field before (control) and during perfusion with 1 mM GABA. Bar, 25 μm. (B) Averaged data showing the time course of $[Na^+]_i$ changes in cultured NG2 cells under control or perfusion with GABA with or without 1 μM TTX. (C) Summary of GABA- and muscimol-induced $[Na^+]_i$ changes in NG2 cells in the presence or absence (control) of various inhibitors. Data were averaged during 3–5 min after the onset of perfusion with 1 mM GABA or 50 μM muscimol, and normalized by the mean fluorescence intensity obtained during the control period (0–5 min before perfusion with GABA or muscimol) for each cell. *, $P < 0.05$; **, $P < 0.01$ compared with the control group or between groups indicated. Error bars represent mean ± SEM.

which indicates the presence of reversal activity of NCX after the muscimol-induced $Na^+$ influx.

### Activation of $GABA_AR$ promotes NG2 cell migration

NG2 cells originating from various brain regions migrate to their destinations during early development (Cameron-Curry and Le Douarin, 1995; Spassky et al., 1998). Because GABAergic signaling plays crucial roles in neural development (Ben-Ari, 2002; Owens and Kriegstein, 2002; Marty and Llano, 2005; Ben-Ari et al., 2007; Di Cristo, 2007; Huang et al., 2007) and $Ca^{2+}$ signaling is critical for directed cell migration (Fay et al., 1995; Komuro and Kumada, 2005; Guan et al., 2007; Manent and Represa, 2007; Zheng and Poo, 2007), we further determined whether the mechanism disclosed above for the GABA-induced $[Ca^{2+}]_i$ elevation is responsible for regulating NG2 cell migration. To address this question, we first used a Boyden transwell chemotaxis assay to assess the migration of purified NG2 cells. We found that application of GABA to the bottom well promoted the chemoattractive migration of NG2 cells, an effect that was blocked by coapplication of bicuculline, TTX, or KB-R7943, but not affected by $GABA_B$ receptor antagonist CGP 55845 (Fig. 8, A and C), which indicates the involvement of $Na^+$ channels and the NCXs, similar to that described above for the GABA-induced $[Ca^{2+}]_i$ elevation.

The GABA-induced increase in the migrated NG2 cells may be caused either by direct chemotaxic effect or by the increased cell mobility. We found that the movement velocity (the accumulated distance of cell movement in all directions over the 60-min imaging period sampled at a rate of 1 image per 5 min) of NG2 cells in the presence of 1 mM GABA (7.86 ± 0.22 μm/h, $n = 40$) was not significantly different from that observed in the absence of GABA (7.59 ± 0.26 μm/h, $n = 25$). Furthermore, NG2 cell migration was not affected by treatment with homogeneous 1 mM GABA applied to both the upper and lower wells of the chamber (Fig. 8 C), which indicates a direct chemotaxic effect of GABA on NG2 cells.

The involvement of $Na^+$ channels and NCXs in the GABA-induced migration of cultured NG2 cells was further confirmed by the siRNA approach. Consistent with the results observed in the GABA-induced $Ca^{2+}$ signaling, we found that GABA-induced migration was blocked in cells transfected either with siNav1.x or with siNCX1, but not affected in cells transfected with scrambled siRNA (Fig. 8, B and C).

Next, we assessed NG2 cell migration from explant culture in response to a GABA gradient created by a GABA-containing agarose block (8 × 8 × 8 $mm^3$) placed adjacent to the explant (Fig. 9 A). A diffusion gradient in the medium surrounding the block was confirmed by fluorescence imaging of Alexa Fluor 488 that was added into the block (Fig. S5). The postnatal SVZ surrounding the lateral ventricles contains OPCs (NG2 cells), and is recognized as a source of forebrain oligodendrocytes in both neonatal (Levison and Goldman, 1993; Spassky et al., 1998) and adult brain (Menn et al., 2006). Dissected SVZ tissue explants from P5–P10 rats were thus cultured for 1 or 2 d before NG2 cell migration was assayed. NG2 cells were identified by post-immunostaining with anti-NG2 antibody. We found a marked increase in NG2 cell populations asymmetrically migrating out of the edge of the explants toward the agarose block containing GABA

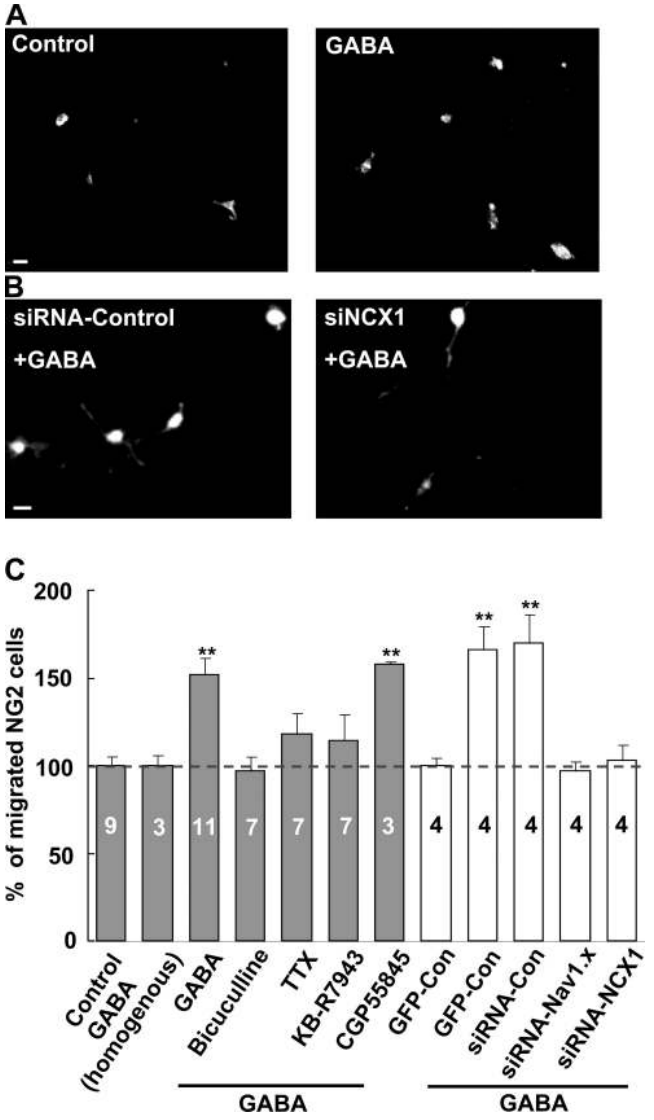


Figure 8. **GABA promoted migration of cultured NG2 cells.** (A) Images showing migrated cells immunopositive for anti-NG2 staining without (control) or with 1 mM GABA added to the bottom chamber of the transwell (see Materials and methods). Bar, 20 µm. (B) Images showing migration of purified NG2 cells cotransfected with pGFP + siRNA-control or pGFP + siRNA-NCX1 in the presence of 1 mM GABA at the bottom chamber of the transwell. Bar, 20 µm. (C) Summary data showing the GABA-induced migration of purified NG2 cells with or without various inhibitors or siRNA transfections. Data are normalized as the percentage of migrated NG2 cells in control (gray) or GFP-control (white) group (broken line; without GABA in the bottom chamber), respectively. Note that homogeneous GABA (1 mM, added in both top and bottom chambers) did not affect NG2 cell migration. **, $P < 0.01$ compared with the control or GFP control group, respectively. Error bars represent mean ± SEM.

(Fig. 9, B–D), with the mean migration distance of NG2 cells in the proximal quadrant (facing the block) much higher than that in the distal quadrant of the explant (Fig. 9 E). The total migration, defined as the number of migrated NG2 cells multiplied by the mean migration distance, was also markedly increased (Fig. 9 F). Moreover, the GABA-induced asymmetric migration was prevented when the agarose blocks contained not only GABA, but also bicuculline, TTX, or KB-R7943 (Fig. 9, D–F). However, GABA still induced chemotactic migration in the presence of $GABA_B$ receptor antagonist CGP 55845 (Fig. 9, D–F).

Cultured brain slice maintains the anatomical organization of the tissue and provides an ideal system for studying mechanisms of cell migration in situ. Gliogenesis mainly takes place in the perinatal period (Levison and Goldman, 1993; Luskin and McDermott, 1994; Zerlin et al., 1995). During the early postnatal period, glial progenitors migrate radially out of the SVZ into the overlying white matter and cortex to develop into astrocytes and oligodendrocytes (Suzuki and Goldman, 2003). To examine whether endogenous GABA affects NG2 cell migration via the mechanism described above, we used cultured neonatal brain slices containing the SVZ and analyzed the effects of various antagonists on the migration of NG2 cells in the SVZ. To identify migrating NG2 cells, a small 1,1′-dioctadecyl-3,3,3′,3′ tetramethylindocarbocyanine (DiI) crystal was deposited in the SVZ after the slice was immunostained live with an anti-NG2 antibody (Fig. 10 A). Migration of DiI-labeled cells out of the DiI-stained area was observed 18–24 h after culturing. Chain migration (Suzuki and Goldman, 2003; Kriegstein and Noctor, 2004; Manent and Represa, 2007) was also observed in some slices (Fig. 10 B). The cell number and the migration distance of the double-labeled cells out of the DiI-stained area were then analyzed. We found that NG2 cells that migrated in the control slices distributed asymmetrically around the DiI-stained area, with more double-labeled cells migrating toward the dorsal–rostral side than those toward the ventral–caudal side of the DiI-stained area (Fig. 10, B, D, and E). This is consistent with previous findings that SVZ progenitors migrated dorsally into the overlying corpus callosum/cortex and rostrally along the rostral migratory stream (Suzuki and Goldman, 2003). In contrast, double-labeled cells in slices treated with bicuculline, TTX, or KB-R7943 migrated more diffusely around the DiI-stained area, with even more apparent migration toward the ventral–caudal side of the DiI-stained area (Fig. 10, C–E).

## Discussion

In the present study, we found that activation of $GABA_AR$ induced membrane depolarization and $[Ca^{2+}]_i$ elevation in NG2 glial cells, a result similar to that found in immature neurons (Ben-Ari, 2002; Owens and Kriegstein, 2002; Ben-Ari et al., 2007). However, the mechanism underlying the $[Ca^{2+}]_i$ elevation induced by activation of $GABA_AR$ in NG2 glial cells was different from that found in immature neurons, where GABA-induced $Ca^{2+}$ entry is mediated by VGCCs and NMDA receptors (Ben-Ari, 2002; Owens and Kriegstein, 2002; Ben-Ari et al., 2007; see Bordey, 2007), whereas $[Ca^{2+}]_i$ elevation in NG2 glial cells is mediated by NCX due to $Na^+$ influx through noninactivating $Na^+$ channels after GABA-induced membrane depolarization (Figs. 3, 4, and 6). It should be noted that the commonly cited mechanistic scheme for GABA's action on neuronal progenitors (i.e., depolarization leading to VGCC opening and calcium entry) has also recently been challenged, and an alternative explanation for calcium entry is required (Bordey, 2007). Interestingly, a persistent $Na^+$ current has been

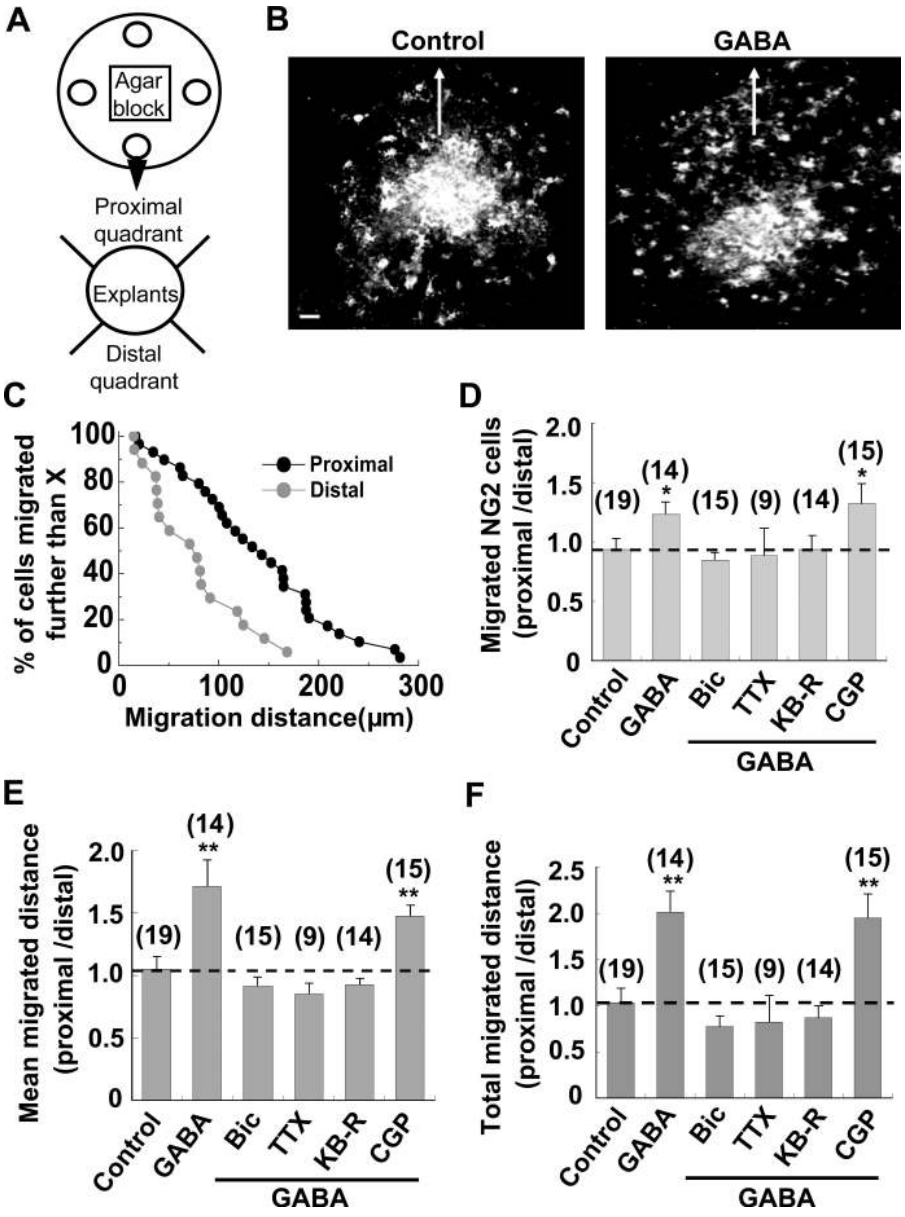


Figure 9. **GABA promoted migration of NG2 cells in tissue explant preparations.** (A) Schematic diagram of the tissue explant migration assay. Four SVZa explants (open circles) were cultured on one poly-D-lysine–coated coverslip. 1 or 2 d after culturing, GABA (50 mM, 50 µl) with or without various inhibitors was added to the well on top of the agarose block (8 mm on a side) sitting in the center of the coverslip to create a concentration gradient of the drugs in the medium surrounding the agarose block. (B) Images of anti-NG2 immunostaining showing the asymmetric or symmetric distribution of NG2 cells migrating from the edge of the explant with or without GABA added to the agarose block. Arrows indicate the direction of the agarose block. Bar, 50 µm. (C) Accumulated distribution of migrated NG2 cells in the proximal and distal quadrants of the SVZa explant in the presence of a GABA-containing agarose block as shown in B. x axis, final distance of migrated NG2 cells from the edge of the explants. y axis, percentage of NG2 cells that migrated further than the distance indicated on the x axis. (D) Averaged ratio (proximal/distal quadrants) of NG2 cells migrating out of explants under various conditions. The number of migrated NG2 cells in the proximal quadrant of the explant was normalized with that in the distal quadrant of the same explant. The number associated with each column represents the number of explants examined. *, $P < 0.05$ compared with control group. (E) Averaged ratio (proximal/distal quadrants) of the mean migration distance of NG2 cells from the edge of explants under various conditions. The mean migration distance of NG2 cells in the proximal quadrant of the explant was normalized with that in the distal quadrant of the same explant. Data were analyzed from the same explants as shown in D. **, $P < 0.01$ compared with control group. (F) Averaged ratio (proximal/distal quadrants) of the total migration distance of NG2 cells from the edge of SVZ explants under various conditions. The summed migration distance of all the NG2 cells in the proximal quadrant of the explant was normalized with that in the distal quadrant of the same explant. Data were analyzed from the same explants as shown in D. **, $P < 0.01$ compared with the control group. Error bars represent mean ± SEM.

shown to be involved in the initiation of giant depolarizing potentials (GDPs) in immature neurons, probably in collaboration with activation of $GABA_A$Rs (Sipilä et al., 2005, 2006). It remains to be explored whether GABA affects functions of neuronal progenitors and immature neurons through a pathway disclosed in the present study in NG2 cells.

Our results indicate that even though $Na^+$ channels expressed in NG2 cells fail to generate typical spikes, $Na^+$ influx itself may play an important role in signal processing through the collaboration with the NCX. Nonspiking neurons are also found in primary sensory systems and in the CNS of invertebrates, where electrotonic spread of local potentials is used effectively for signal transmission (Juusola et al., 1996). The graded membrane depolarization causes graded and continuous transmitter release by increased $[Ca^{2+}]_i$ through activation of VGCCs (Juusola et al., 1996; Wilson, 2004), and has been found to be an efficient form for transmitting information (Juusola et al., 1996). The short cytoplasmic processes and high input resistance in NG2 cells may permit these cells even more effective electrotonic spread of local potentials than neurons. Thus, the collaboration of noninactivating voltage-gated $Na^+$ channels and NCXs in NG2 cells found in the present study provides a unique mechanism for $[Ca^{2+}]_i$ elevation that may be crucial for graded signal processing in these cells. It will be of interest to determine whether a similar $Na^+$ channel–NCX pathway contributes to the analogue coded signal transmission in nonspiking neurons.

During the early stage of brain development, GABA becomes functional before synapse formation. Tonic as well as phasic nonsynaptic release of GABA from neural progenitors and immature neurons may play an important role in neural development (Vautrin et al., 2000; Nguyen et al., 2001; Liu et al., 2005; Bordey, 2007; Wu et al., 2007). Our results indicate that

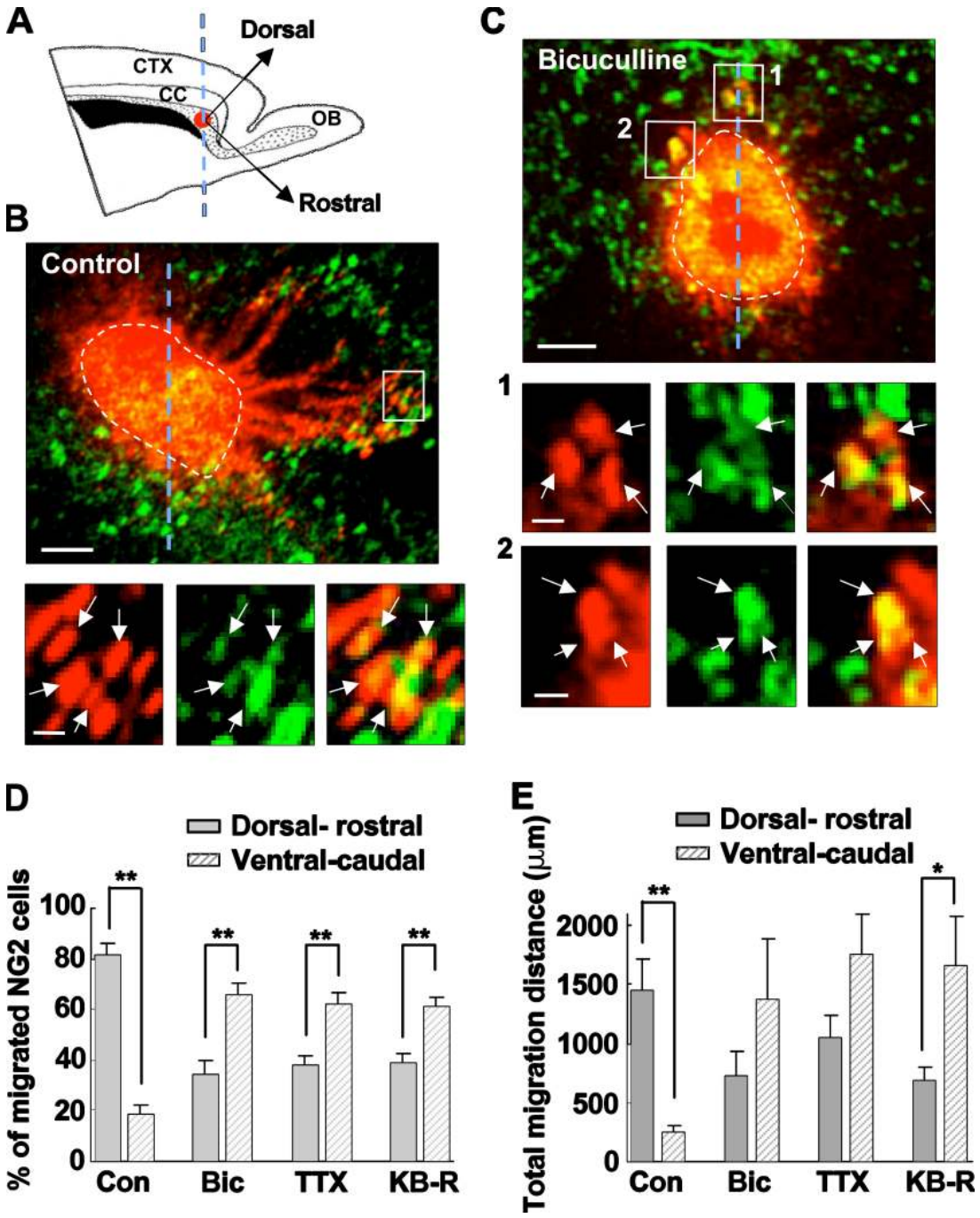


Figure 10. **Involvement of endogenous GABA in the in situ migration of SVZ NG2 cells.** (A) Schematic representation of the rat sagittal brain slice showing the location of DiI-stained area (red circle) in the SVZ (gray area). Two arrows indicate the rostral direction (starting from the center of the DiI-stained area and along the longitude axis of the SVZ to the olfactory bulb direction) and dorsal direction (perpendicular with the rostral direction), respectively. The broken blue line crossing the center of the DiI-stained area and forming 45° angles with the two arrows separates the DiI-stained area into the dorsal–rostral (the right side of the broken blue line) and ventral–caudal (the left side of the broken blue line) parts for analyzing cell migration (see below). CC, corpus callosum; CTX, cortex; OB, olfactory bulb. (B, top) Confocal image of the control slice 18 h after live staining with anti-NG2 (green) and DiI crystal (red) showing asymmetric distribution of DiI-labeled cells around the DiI-stained area (outlined by the broken line). Note that more DiI-stained cells, either NG2 positive or NG2 negative, migrated out of the DiI-stained area in the dorsal–rostral side (the right side of the broken line) than those in the ventral–caudal side (the left side of the broken line). Bar, 100 μm. (B, bottom) Higher magnification of the boxed area in the top panel showing that NG2 cells (stained with both DiI and anti-NG2, indicated by arrows) migrated out of the DiI-stained area. Bar, 20 μm. (C, top) Confocal image of the bicuculline-treated slice 18 h after live staining with anti-NG2 (green) and DiI crystal (red) showing symmetric distribution of DiI-labeled cells around the DiI-stained area (outlined by the broken line). Bar, 100 μm. (middle and bottom) Higher magnification of the boxed areas 1 and 2 in the top panel, respectively, showing that double-stained NG2 cells (indicated by arrows) migrated out of the DiI-stained area. Bars, 20 μm. (D) Averaged ratio (number of the migrated NG2 cells in one side/total number of the migrated NG2 cells) of NG2 cells migrating out of the DiI-stained area in the absence (control) or presence of 10 μM bicuculline (Bic), 1 μM TTX, or 10 μM KB-R7943 (KB-R). (E) Averaged total migration distance of NG2 cells (summed migration distance from all the migrated NG2 cells in one side) starting from the edge of the DiI-stained area under various conditions. Data were analyzed from the same brain slices as shown in D. *, $P < 0.05$; **, $P < 0.01$ compared between the two groups indicated. $n$ = 23, 13, 9, and 11 slices for control, bicuculline, TTX, and KB-R7943 groups, respectively. Error bars represent mean ± SEM.

GABA may also function as an important signaling molecule for migration of glial precursors, although the pathway mediating GABA-induced NG2 cell migration after activation of $GABA_A$Rs, which involves $Na^+$ channels and NCXs, may be distinguished from that mediating the GABA-induced neuronal migration, which may involve $Ca^{2+}$ channels (Behar et al., 1996, 1998; Ben-Ari, 2002; Owens and Kriegstein, 2002; Ben-Ari et al., 2007; Akerman and Cline, 2007; see Bordey, 2007). Interestingly, blockage of NCXs has been found to impair cell migration in microglia (Ifuku et al., 2007) and MDCK-F cells (Dreval et al., 2005), although the pathway leading to the activation of NCXs in these cells is not clear. Our results, obtained by the siRNA approach, suggest that GABA-induced $Ca^{2+}$ signaling and migration of NG2 cells are mediated mainly through the NCX1 subtype of NCXs.

A gradient of low-to-high immunoreactivity for GABA is observed from the ventricular zone to the cortical plate of the developing telencephalon (Heng et al., 2007), which suggests the involvement of endogenous GABA signaling in directional cortical neuronal migration (Ben-Ari, 2002; Represa and Ben-Ari, 2005; Ben-Ari et al., 2007; Heng et al., 2007; Manent and Represa, 2007) and NG2 cell migration (Fig. 10) from the SVZ. Similar to the case of neuronal progenitors (Vautrin et al., 2000; Nguyen et al., 2001; Liu et al., 2005; Bordey, 2007), tonic and phasic membrane depolarizations induced by endogenously released GABA were recorded in NG2 cells in slice preparations. Spontaneous GDPs resulted from synchronized GABA release have been recorded in the vast majority of neurons in the neonatal brain, and may play important roles in neural development (Sipilä et al., 2005, 2006; Ben-Ari et al., 2007; Bordey, 2007). Although we did not record typical GDP, probably because of the limited recording period and cell numbers examined, we did recorded spontaneous phasic GABA currents in NG2 cells from brain slices (Fig. 2 C; see Lin and Bergles, 2004a). Such synchronous phasic GABA release may reach a relatively high concentration locally near NG2 cells. Because of its high membrane resistance, activation of relatively few $GABA_A$R in the NG2 cell membrane may be sufficient to open $Na^+$ channels. Furthermore, GABA may act together with other depolarization-inducing factors, including excitatory neurotransmitters released by other cells, elevated extracellular $K^+$ concentration accompanying high neuronal activity, activation of mechanical sensitive channels due to the osmotic load induced by chloride entry (Marty and Llano, 2005) or morphological changes during cell growth and migration, and pH change after $GABA_A$R activation and $HCO_3$ flux that may affect transient receptor potential channels (Ryu et al., 2007).

The finding that bicuculline, TTX, and KB-R7943 are all effective in blocking the directional migration of NG2 cells in cultured brain slices (Fig. 10) suggests that endogenous GABA may be functional in inducing NG2 cell migration through activation of the $GABA_A$R–$Na^+$ channel–NCX pathway. However, the possibility also exists that bicuculline may indirectly affect NG2 cell migration in slices due to its effects on other neural cells expressing $GABA_A$Rs. To exclude this possibility, further studies will be needed using approaches to specifically knock out $GABA_A$Rs on NG2 cells in vivo. It should be pointed out that the pathway disclosed in the present study may not be limited to GABA. Any ligand that induces sufficient membrane depolarization in NG2 cells may elevate $[Ca^{2+}]_i$ by activating the $Na^+$ channel–NCX pathway and induce NG2 cell migration by triggering the $Ca^{2+}$-dependent mechanisms required for cell migration, including cytoskeletal reorganization, cell mobility, membrane traffic, and cell adhesion and de-adhesion (Komuro and Kumada, 2005; Guan et al., 2007; Manent and Represa, 2007; Zheng and Poo, 2007).

Glutamate release induced by the $Na^+$ channel opener veratridine has been related with the NCX pathway in mouse neocortical preplate neurons (Platel et al., 2005). It is unclear whether NG2 cells can modulate neuronal activity by releasing signaling molecules through a similar $Na^+$ channel–NCX pathway in response to GABAergic synaptic activity. However, the $Na^+$ channel–NCX pathway has been implicated in anoxic injury of CNS white matter (Stys et al., 1992, 1993; Rosenberg et al., 1999). Furthermore, increased neuronal coexpression of NCXs and the Nav1.6 type of $Na^+$ channel has been related to the pathogenesis of multiple sclerosis (Craner et al., 2004; Waxman et al., 2004; Rush et al., 2005). The $Ca^{2+}$ entry through the noninactivating $Na^+$ channel–NCX pathway in NG2 cells may thus be important for both physiological and pathological processes.

## Materials and methods

### Slice preparation

The use and care of animals followed the guidelines of the Shanghai Institutes of Biological Sciences Animal Research Advisory Committee. Sprague-Dawley (SD) rats (P7–P32) were anesthetized with sodium pentobarbital. After decapitation, the hippocampal formation was dissected rapidly and placed in ice-cold oxygenated (95% $O_2$/5% $CO_2$) artificial cerebrospinal fluid (ACSF) containing 110 mM choline chloride, 2.5 mM KCl, 0.5 mM $CaCl_2$, 7 mM $MgCl_2$, 1.3 mM $NaH_2PO_4$, 0.6 mM sodium pyruvate, and 1.3 mM sodium ascorbic acid (Zhang et al., 2003). Transverse slices (250–400-µm thick) were cut with a vibratome (HM 650 V; Thermo Fisher Scientific) and bubbled in normal solution for at least 1 h at room temperature (~26°C) containing 119 mM NaCl, 2.5 mM KCl, 2.5 mM $CaCl_2$, 1.3 mM $MgCl_2$, 1 mM $NaH_2PO_4$, 26.2 mM $NaHCO_3$, and 11 mM D-glucose. During the experiments, slices were visualized under a microscope (BX51WI; Olympus) using infrared video microscopy (U-CMAD-2; Olympus) and differential interference contrast optics.

### Freshly dissociated NG2 cell preparation

Brain cortex slices were prepared from postnatal 3–4-d-old (P3–P4) SD rats and maintained in ACSF solution containing 125 mM NaCl, 2.5 mM KCl, 2 mM $CaCl_2$ × 2 mM $H_2O$, 1.3 mM $MgCl_2$ × 6 mM $H_2O$, 1.3 mM $NaH_2PO_4$ × 2 mM $H_2O$, 25 mM $NaHCO_3$, and 10 mM glucose (bubbled with 95% $O_2$–5% $CO_2$ for 1 h). Subsequently, the slices (two to three from each animal) were transferred into standard ACSF solution containing 4.4 U/ml papain and 0.6 mM L-cysteine, and bubbled with 95% $O_2$–5% $CO_2$ at 22°C for 20 min. After the enzyme digestion, the slices were washed three or four times in L-15 medium (Invitrogen) with 5% FBS and triturated through flame-polished pipettes onto poly-D-lysine–coated coverslips, then allowed to adhere for 2–3 h before surface immunostaining (see Immunocytochemistry) and sequential calcium imaging experiments.

### Cell cultures

Purified NG2 cells were isolated by two passages as described by Itoh (2002), with some modifications. In brief, embryonic day 16 (E16) SD rat embryonic cortex was mechanically dissociated and suspended through 20-µm-pore sterile nylon mesh, plated on poly-D-lysine–coated 100-mm-diameter culture dishes (Corning) at a density of $3 \times 10^7$ cells/dish, cultured with MEM (Invitrogen) containing 10% FBS, and maintained at 37°C in a 5% $CO_2$ incubator. After incubation for 5 d, the cells were passaged with 0.05% trypsin in EDTA (first passage), resuspended, and finally sieved through 20-µm-pore nylon mesh. The dispersed cells were seeded on

noncoated 60-mm-diameter culture dishes at a density of $8 \times 10^6$ cells/dish containing 10% FBS in MEM. After another 6 d of incubation, the cells were passaged with 0.025% trypsin in EDTA (second passage) and dispersed on noncoated coverslips at a density of $10^6$ cells/dish in the same medium. All experiments were performed 1–2 d after the second passaging of NG2 cells.

**siRNA and transfection**

The siRNAs used in this study were designed as described previously (Slodzinski and Blaustein, 1998; Xu and Shrager, 2005). In brief, siRNA (5′-AAGCAUGUUGUACAAUGAG-3′) specifically targeted to the start codon region of NCX1 mRNA were synthesized (Slodzinski and Blaustein, 1998). To knock down multiple rat $Na^+$ channel subtypes, the sequence of the sense strand of 19 nucleotides 5′-GTTCGACCCTGACGCCACT-3′ was chosen (Xu and Shrager, 2005). Scrambled siRNA, 5′-UUCUCCGAACGUGUCACGU-3′, which targets a nonmammalian gene, was used as the stable negative control. The purified NG2 cells were plated on 35-mm culture dish 6 h before transfection. For identification and knockdown efficiency analysis, a plasmid expressing enhanced GFP (pGFP) was cotransfected with siRNA at the ratio of 1:2 using Lipofectamine 2000 (Invitrogen), as described previously (Hahn et al., 2007; Barker and Diamond, 2008). Typically, 1 µg of GFP plasmid and 2 µg of siRNA were mixed with 2 µl Lipofectamine, added to each 35-mm culture dish, and incubated at 37°C for 2 h before washing.

**Electrophysiological recordings**

For whole cell recordings from brain slices, NG2 glial cells were visualized using an upright microscope (BX51WI) equipped with a LUMPlanFI/IR 40×/0.8 W objective and an infrared charge-coupled device (U-CMAD-2; all from Olympus). Recordings were made with Axon MultiClamp 700A patch-clamp amplifiers (MDS Analytical Technologies) at room temperature. Persistent $Na^+$ currents were recorded with a patch electrode (6–9 MΩ tip resistance) and filtered at 2 kHz. For phenytoin-induced persistent $Na^+$ current, the internal solution contained 125 mM Cs-gluconate, 10 mM Hepes, 10 mM EGTA, 2 mM $MgCl_2 \times 6$ mM $H_2O$, 1 mM $CaCl_2 \times 2$ mM $H_2O$, 4 mM $Na_2$-ATP, and 0.5 mM $Na_3$-GTP, pH 7.3, with CsOH). The oxygenated bath solution contained 120 mM NaCl, 20 mM tetraethylammonium (TEA)-Cl, 2 mM KCl, 4 mM $MgCl_2 \times 6$ mM $H_2O$, 1 mM $CaCl_2 \times 2$ mM $H_2O$, 2 mM 4-AP, 16 mM $NaHCO_3$, 10 mM D-glucose, 0.1 mM $CdCl_2$, 0.5 mM $NiCl_2$, and 0.1 mM phenytoin. For riluzole-induced persistent $Na^+$ current, the internal solution contained mM 125 Cs-gluconate, 10 mM Hepes, 0.2 mM EGTA, 10 mM TEA-Cl, 2 mM MgATP, 0.3 mM $Na_3$-GTP, and 10 mM $Na_2$-phosphocreatine, pH 7.2, with CsOH. The oxygenated bath solution contained 80 mM NaCl, 40 mM CsCl, 3 mM KCl, 2 mM $MgCl_2$, 2 mM $CaCl_2$, 0.1 mM $CdCl_2$, 2 mM 4-AP, 2 mM $CoCl_2$, 1 mM $BaCl_2$, 26 mM $NaHCO_3$, 11 mM D-glucose, and 0.01 mM riluzole.

Gramicidin perforated-patch recordings in NG2 slices were obtained using a final gramicidin concentration of 20–30 µg/ml of pipette solution (prepared from a stock solution of 1 mg/ml in DMSO) containing 143 mM potassium gluconate, 2 mM KCl, 10 mM Hepes, and 0.5 mM EGTA.

Patch recordings for cultured NG2 cells were made at room temperature using an EPC9 patch clamp amplifier driven by PatchMaster software, version 2.01 (HEKA). Cells were visualized using a phase-contrast inverted microscope (IX50; Olympus) equipped with an LCAch 20×/0.4 PhC objective (Olympus). Voltage-dependent $Na^+$ and $Ca^{2+}$ currents were recorded with a patch electrode (7–10 MΩ tip resistance) in whole-cell recording mode and filtered at 2 kHz. The pipette solution contained 135 mM CsCl, 10 mM TEA-Cl, 3 mM $MgCl_2 \times 6$ mM $H_2O$, 10 mM EGTA, 10 mM Hepes, 3 mM Mg-ATP, and 0.3 mM Na-GTP (adjusted to pH 7.2 with CsOH, 310 mOsm). The conventional ECS contained 145 mM NaCl, 3 mM KCl, 2 mM $MgCl_2 \times 6$ mM $H_2O$, 3 mM $CaCl_2 \times 2$ mM $H_2O$, 10 mM Hepes, and 8 mM D-glucose. The ECS for $Na^+$ channel recordings was a Hepes-buffered saline containing 60 mM CsCl, 30 mM NaCl, 20 mM TEA-Cl, 1 mM $BaCl_2 \cdot 2H_2O$, 2 mM 4-AP, 2 mM $MgCl_2 \cdot 6H_2O$, 45 mM choline chloride, 0.1 mM $CdCl_2$, 10 mM Hepes, and 10 mM D-glucose (pH 7.3 with NaOH, 310 mOsm). The ECS for $Ca^{2+}$ channel recordings was a Hepes-buffered saline containing 60 mM CsCl, 50 mM NaCl, 20 mM TEA-Cl, 20 mM$BaCl_2 \times 2$ mM $H_2O$, 2 mM 4-AP, 2 mM $MgCl_2 \times 6$ mM $H_2O$, 0.0005 mM TTX, 10 mM Hepes, and 10 mM D-glucose, pH 7.3.

The recorded membrane potentials were corrected by the calculated liquid junction potentials, which are 12.5 mV (for the riluzole experiment) and15.3 mV (for the phenytoin experiment) for whole-cell patch recording of $Na^+$ currents, and 15 mV for gramicidin perforated-patch recordings in brain slices. We did not detect a sudden change in recorded membrane potential when we deliberately made a break into whole cell recordings from gramicidin perforated-patch recordings, which is consistent with previous observation that the "patch potential" does not exist in gramicidin patch recordings when the pipette was filled with potassium gluconate (Kim and Trussell, 2007). Because perforated-patch recordings tend to have high access resistance (30–50 MΩ in the present study) that may cause significant voltage drop across the pipette when they pass through a large current, the actual membrane potentials (Vm) clamped for estimation of GABA reversal potential were also corrected for access resistance (*Ra*) according to Vm = Vh − Ih × Ra, where Vh is the holding potential and Ih is the current applied through the pipette at the holding potential (Zhang et al., 2006).

**Calcium imaging**

For $Ca^{2+}$ imaging of brain slices, slices were loaded with Fluo4-AM (3–5 µM; Invitrogen) for 1 h after surface immunostaining with mouse monoclonal antibody against NG2 at 25°C. For $Ca^{2+}$ imaging in freshly isolated cells, cells were loaded with Fluo4-AM (3–5 µM) for 20–30 min in conventional ECS after surface immunostaining with mouse monoclonal antibody against NG2 in a 37°C incubator. Purified NG2 cells were loaded with 1 µM Fluo-4 AM or 5 µM Rhod2-AM (Invitrogen) in culture medium for 40 or 30 min, respectively, in an incubator. The cells were then washed with conventional ECS and imaged with 488-nm excitation and a 500-nm long-pass barrier filter for Fluo4-AM and 540 nm excitation for Rhod2-AM, with a laser confocal microscope (IX71; Olympus) using a 60×/1.2 W or 20×/0.7 UPlan-Apochromat objective lens (Olympus) at a resolution of 512 × 512. A low laser power (<0.5%) was used to avoid possible fluorescence bleaching. The fluorescent images were collected every 5 s and analyzed using Fluoview 500 software (Olympus). For $Na^+$-free experiments, the NaCl in ECS was replaced with choline chloride.

**Sodium imaging**

Sodium imaging was done with SBFI/AM (Invitrogen; Rose et al., 1998). Cultured NG2 cells were loaded with 5 µM SBFI/AM (10 mM stock solution mixed with an equal volume of 20% [wt/vol] pluronic F-127 [Sigma-Aldrich] in DMSO) for 45 min at 37°C. The perfusion chamber was placed on the stage of a TE2000-E Diaphot inverted microscope (Nikon) equipped with a 40×/1.3 oil immersion objective (Nikon) and driven by MetaFluor software (MDS Analytical Technologies). The fluorescence ratio was monitored at excitation wavelengths of 340 and 380 nm, and detection of emission was monitored at 500 nm. The fluorescent images were collected every 6 s and analyzed using Metamorph software.

**Immunocytochemistry**

For conventional immunostaining, cultured cells were fixed by 4% paraformaldehyde in PBS at 4°C for 20 min and were permeabilized with 0.2% Triton X-100 in PBS for 10 min (Zhang et al., 2007). Primary antibody against NG2 (1:300; Millipore), $PDGF_\alpha$ receptor (1:50; Cell Signaling Technology), β-III tubulin (1:1,000; Promega), GFAP (1:500; Dako), CD11b (1:50; BD), NCX1 (1:200; Swant), NCX2 (1:100; Santa Cruz Biotechnology, Inc.), and Pan Nav (1:200; Alomone Labs) were applied overnight, respectively, at 4°C, followed by rinses in PBS and staining with Cy3 (1:1,000) or Alexa Flour 488–conjugated secondary antibodies (1:1,000; Invitrogen) at room temperature. Images were collected with the laser confocal microscope (IX71) using a 60×/1.2 W objective (Olympus) driven by Fluoview 500 software and taken at a resolution of 512 × 512. The gain of the photomultiplier was adjusted to maximize the signal/noise ratio without causing saturation by the strongest signals.

**Live immunofluorescent staining**

Acutely dissociated hippocampal cells were incubated with rabbit polyclonal antibody against NG2 (1:200; Millipore) at 37°C in ECS for 7–10 min. After three washes with ECS, cells were incubated with CY3-conjugated goat anti–rabbit antibody (1:1,000; Jackson ImmunoResearch Laboratories) for another 4–5 min at room temperature, followed by three washes in ECS. Cells were then maintained in ECS in a recording chamber for calcium imaging experiments.

For live immunostaining in brain slices, the slices were incubated in oxygenated (95% $O_2$/5% $CO_2$) ACSF with anti–mouse NG2 antibody (1:200; Millipore) at room temperature for 1 h. After three gentle washes with ACSF, slices were incubated in oxygenated ACSF with CY3-conjugated goat anti–mouse antibody (Jackson ImmunoResearch Laboratories) at 1:800 for another 30 min at room temperature followed by washes with ACSF. The slices were then bubbled in normal solution in a recording chamber for calcium imaging experiments.

**Cell migration assay**

Migration of purified OPC cells was assayed using a Boyden microchemotaxis chamber system (5 µm pore size; Corning). The cells were seeded in the upper insert of a chamber at $1 \times 10^5$ cells per well. In the bottom well,

250 µl of MEM with 10% FBS with or without other reagents was added. 2 d after seeding, cells were fixed with 4% paraformaldehyde, and non-migrated cells were removed from the top compartment with a cotton swab. Cells attached to the bottom side of the membranes were immunostained with the anti-NG2 antibody. For cultures transfected with GFP with or without siRNAs, the GFP-positive migrated cells were counted in the bottom side of the transwell membrane. Cells were analyzed directly under a confocal microscope (IX71) equipped with a 20× /0.7 UPlan-Apochromat objective lens (Olympus) driven by Fluoview 500 software. Each condition was run in 4–9 wells in each assay. For cell mobility assessment, cells were imaged every 5 min, and the accumulated movement distance of a cell over 60 min imaging period was calculated.

**Tissue explant culture**

Brains from P5–P10 SD rats were cut in ACSF with a vibratome. Sagittal sections of tissue within the borders of the SVZ were dissected out to make SVZa explants of 200–400 µm in diameter (Wu et al., 1999). Four SVZa explants were cultured on one poly-D-lysine–coated coverslip in DME/F12 (1:1) supplemented with 10% FBS and penicillin. 1 or 2 d after culture, a 4% agarose block (8 mm on a side) was put at the center of the coverslip. GABA (50 mM, 50 µl) was added to a small well (3 mm in diameter) on the top of the agarose block. A diffusion gradient in the medium surrounding the block was detectable as early as 1 h after the drug was added to the block, and was maintained as long as 24 h, as assayed by fluorescence imaging of Alexa Fluor 488 (Fig. S5; see Zheng et al., 1994), which was added to the well in the block (5 µM, 50 µl). The concentration of the dye was estimated to be ~50–500 times diluted in the medium surrounding the block, depending on the distance from the edge of the block and the time after the dye was added to the small well. In some experiments, 50 µl of one of the following inhibitors was also added to the small well to determine the mechanisms of GABA-induced migration: 500 µM bicuculine, 50 µM TTX, 100 µM KB-R7943, and 250 µM CGP 55845. After being cultured for another day, all the explants were fixed with 4% paraformaldehyde and immunostained with anti-NG2 antibody. Migratory NG2 cells surrounding explants were imaged by a laser confocal microscope (IX71) with Fluoview 500 using a 60×/1.2 or 20×/0.7 UPlan-Apochromat objective lens (Olympus) and analyzed with ImageJ software.

**In situ NG2 cell migration assay in brain slice cultures**

SD pups at P0–P3 were anesthetized, and medial sagittal sections at the level of the septal nuclei and the rostral migratory stream were cut at 300-µm thickness with a vibratome (Suzuki and Goldman, 2003). The slices were separated and transferred to sterile, porous membrane units (0.4 µm; Millicell-CM; Millipore). The units were placed into 6-well trays containing 1 ml of culturing medium in each well with DME/F12 (1:1) supplemented with 10% fetal bovine serum and penicillin. After recovery for 1 h, the slices were made for live surface immunostaining with anti–mouse NG2 antibody (1:200; Millipore) and Alexa Fluor 488–conjugated secondary antibody (1:800; Invitrogen) for 1 h and 45 min at 37°C in a 5% $CO_2$ incubator, respectively. To identify migrating NG2 cells, small crystals of DiI (Sigma-Aldrich) were deposited in anterior SVZ with the help of a dissecting scope after immediately executed live immunostaining (Soria and Valdeolmillos, 2002). After culturing for 18–24 h, the double-labeled sections were fixed with 4% paraformaldehyde for 3 h and viewed by a laser-scanning confocal microscope (LSM510; Carl Zeiss, Inc.), and three-dimensional reconstructions of z series images were performed with Plan-Neofluar 5×/0.15 Ph1 and Achroplan 20×/0.5 W Ph2 objective lenses at room temperature. The images were collected and analyzed by the LSM image browser and ImageJ software.

**Drug application**

For studying GABA-induced current or depolarization, a miniature Y tube was used to allow rapid and localized application of drug-containing saline to the cell recorded (Duan and Cooke, 2000). For imaging studies of GABA-induced elevation of $[Ca^{2+}]_i$ or $[Na^+]_i$, the perfusion system for the whole recording chamber was used to allow drug application to a large population of cells.

**Statistics**

All electrophysiological data were analyzed by Clampfit 9.0 software (MDS Analytical Technologies). All data are presented as mean ± SEM. Statistical comparisons were assessed with an ANOVA test or unpaired *t* test; $P < 0.05$ was taken as significant.

**Online supplemental material**

Fig. S1 shows the purity of cultured NG2 cells identified by immunostaining. Fig. S2 shows the expression of NCX1 and NCX2 in neurons and NG2 cells in rat cortical slices. Fig. S3 shows apparent expression of NCX1 but not NCX2 in cultured NG2 cells. Fig. S4 shows siRNA knockdown of NCX1 and $Na^+$ channels in cultured NG2 cells. Fig. S5 shows the diffusion gradient in the medium surrounding the agarose block. Video 1 shows the GABA-induced $[Ca^{2+}]_i$ elevation in NG2 cells in hippocampal slices. Video 2 shows the GABA-induced $[Ca^{2+}]_i$ elevation in cultured NG2 cells. Online supplemental material is available at http://www.jcb.org/cgi/content/full/jcb.200811071/DC1.

We thank Dr. M.-m. Poo and Dr. Iain Bruce for critical reading the manuscript, and Dr. X.-B. Yuan, X.-J. Yang, Q. Hu, J.-B. Mao, and X.-M. Wu for technical assistance.

This work was supported by grants from the Major State Basic Research Program of China (2006CB806600), the National Natural Science Foundation of China (30730037), the Chinese Academic Sciences (KSCX2-YW-R-101), and the Science and Technology Commission of Shanghai Municipality (07XD14039).

Submitted: 14 November 2008
Accepted: 16 June 2009

## References

Aguirre, A., J.L. Dupree, J.M. Mangin, and V. Gallo. 2007. A functional role for EGFR signaling in myelination and remyelination. *Nat. Neurosci.* 10:990–1002.

Akerman, C.J., and H.T. Cline. 2007. Refining the roles of GABAergic signaling during neural circuit formation. *Trends Neurosci.* 30:382–389.

Annunziato, L., G. Pignataro, and G.F. Di Renzo. 2004. Pharmacology of brain $Na^+/Ca^{2+}$ exchanger: from molecular biology to therapeutic perspectives. *Pharmacol. Rev.* 56:633–654.

Barker, G.A., and S.L. Diamond. 2008. RNA interference screen to identify pathways that enhance or reduce nonviral gene transfer during lipofection. *Mol. Ther.* 16:1602–1608.

Barres, B.A., W.J. Koroshetz, K.J. Swartz, L.L. Chun, and D.P. Corey. 1990. Ion channel expression by white matter glia: the O-2A glial progenitor cell. *Neuron.* 4:507–524.

Behar, T.N., Y.X. Li, H.T. Tran, W. Ma, V. Dunlap, C. Scott, and J.L. Barker. 1996. GABA stimulates chemotaxis and chemokinesis of embryonic cortical neurons via calcium-dependent mechanisms. *J. Neurosci.* 16:1808–1818.

Behar, T.N., A.E. Schaffner, C.A. Scott, C. O'Connell, and J.L. Barker. 1998. Differential response of cortical plate and ventricular zone cells to GABA as a migration stimulus. *J. Neurosci.* 18:6378–6387.

Ben-Ari, Y. 2002. Excitatory actions of GABA during development: the nature of the nurture. *Nat. Rev. Neurosci.* 3:728–739.

Ben-Ari, Y., J.L. Gaiarsa, R. Tyzio, and R. Khazipov. 2007. GABA: a pioneer transmitter that excites immature neurons and generates primitive oscillations. *Physiol. Rev.* 87:1215–1284.

Bergles, D.E., J.D. Roberts, P. Somogyi, and C.E. Jahr. 2000. Glutamatergic synapses on oligodendrocyte precursor cells in the hippocampus. *Nature.* 405:187–191.

Blakemore, W.F., and H.S. Keirstead. 1999. The origin of remyelinating cells in the central nervous system. *J. Neuroimmunol.* 98:69–76.

Blaustein, M.P., and W.J. Lederer. 1999. Sodium/calcium exchange: its physiological implications. *Physiol. Rev.* 79:763–854.

Bordey, A. 2007. Enigmatic GABAergic networks in adult neurogenic zones. *Brain Res. Brain Res. Rev.* 53:124–134.

Brickley, S.G., S.G. Cull-Candy, and M. Farrant. 1996. Development of a tonic form of synaptic inhibition in rat cerebellar granule cells resulting from persistent activation of GABAA receptors. *J. Physiol.* 497:753–759.

Brumback, A.C., and K.J. Staley. 2008. Thermodynamic regulation of NKCC1-mediated $Cl^-$ cotransport underlies plasticity of GABA(A) signaling in neonatal neurons. *J. Neurosci.* 28:1301–1312.

Butt, A.M., J. Kiff, P. Hubbard, and M. Berry. 2002. Synantocytes: new functions for novel NG2 expressing glia. *J. Neurocytol.* 31:551–565.

Cameron-Curry, P., and N.M. Le Douarin. 1995. Oligodendrocyte precursors originate from both the dorsal and the ventral parts of the spinal cord. *Neuron.* 15:1299–1310.

Chang, A., A. Nishiyama, J. Peterson, J. Prineas, and B.D. Trapp. 2000. NG2-positive oligodendrocyte progenitor cells in adult human brain and multiple sclerosis lesions. *J. Neurosci.* 20:6404–6412.

Cherubini, E., J.L. Gaiarsa, and Y. Ben-Ari. 1991. GABA: an excitatory transmitter in early postnatal life. *Trends Neurosci.* 14:515–519.

Chittajallu, R., A. Aguirre, and V. Gallo. 2004. NG2-positive cells in the mouse white and grey matter display distinct physiological properties. *J. Physiol.* 561:109–122.

Craner, M.J., J. Newcombe, J.A. Black, C. Hartle, M.L. Cuzner, and S.G. Waxman. 2004. Molecular changes in neurons in multiple sclerosis: altered axonal expression of Nav1.2 and Nav1.6 sodium channels and $Na^+/Ca^{2+}$ exchanger. *Proc. Natl. Acad. Sci. USA.* 101:8168–8173.

Di Cristo, G. 2007. Development of cortical GABAergic circuits and its implications for neurodevelopmental disorders. *Clin. Genet.* 72:1–8.

Dreval, V., P. Dieterich, C. Stock, and A. Schwab. 2005. The role of $Ca^{2+}$ transport across the plasma membrane for cell migration. *Cell. Physiol. Biochem.* 16:119–126.

Duan, S., and I.M. Cooke. 2000. Glutamate and GABA activate different receptors and $Cl^-$ conductances in crab peptide-secretory neurons. *J. Neurophysiol.* 83:31–37.

Fay, F.S., S.H. Gilbert, and R.A. Brundage. 1995. Calcium signalling during chemotaxis. *Ciba Found. Symp.* 188:121–135.

Franklin, R.J. 2002. Why does remyelination fail in multiple sclerosis? *Nat. Rev. Neurosci.* 3:705–714.

Ge, W.P., X. Yang, Z. Zhang, H. Wang, W. Shen, Q. Deng, and S. Duan. 2006. Long-term potentiation of neuron-glia synapses mediated by $Ca^{2+}$-permeable AMPA receptors. *Science.* 312:1533–1537.

Guan, C.B., H.T. Xu, M. Jin, X.B. Yuan, and M.M. Poo. 2007. Long-range $Ca^{2+}$ signaling from growth cone to soma mediates reversal of neuronal migration induced by slit-2. *Cell.* 129:385–395.

Hahn, P., G. Niemann, A. Grewe, and W. Bielke. 2007. An siRNA-based system for differential regulation of ectopic gene expression constructs. *J. Biotechnol.* 128:762–769.

Heng, J.I., G. Moonen, and L. Nguyen. 2007. Neurotransmitters regulate cell migration in the telencephalon. *Eur. J. Neurosci.* 26:537–546.

Huang, Z.J., F. Ango, and G. Di Cristo. 2007. Development of GABA innervation in cerebral and cerebellar cortices. *Nat. Rev. Neurosci.* 8:673–686.

Ifuku, M., K. Färber, Y. Okuno, Y. Yamakawa, T. Miyamoto, C. Nolte, V.F. Merrino, S. Kita, T. Iwamoto, I. Komuro, et al. 2007. Bradykinin-induced microglial migration mediated by B1-bradykinin receptors depends on $Ca^{2+}$ influx via reverse-mode activity of the $Na^+/Ca^{2+}$ exchanger. *J. Neurosci.* 27:13065–13073.

Itoh, K. 2002. Culture of oligodendrocyte precursor cells ($NG2^+$ /$O1^-$) and oligodendrocytes ($NG2^-$ /$O1^+$) from embryonic rat cerebrum. *Brain Res. Brain Res. Protoc.* 10:23–30.

Juusola, M., A.S. French, R.O. Uusitalo, and M. Weckstrom. 1996. Information processing by graded-potential transmission through tonically active synapses. *Trends Neurosci.* 19:292–297.

Káradóttir, R., P. Cavelier, L.H. Bergersen, and D. Attwell. 2005. NMDA receptors are expressed in oligodendrocytes and activated in ischaemia. *Nature.* 438:1162–1166.

Káradóttir, R., N.B. Hamilton, Y. Bakiri, and D. Attwell. 2008. Spiking and nonspiking classes of oligodendrocyte precursor glia in CNS white matter. *Nat. Neurosci.* 11:450–456.

Keirstead, H.S., T. Ben-Hur, B. Rogister, M.T. O'Leary, M. Dubois-Dalcq, and W.F. Blakemore. 1999. Polysialylated neural cell adhesion molecule-positive CNS precursors generate both oligodendrocytes and Schwann cells to remyelinate the CNS after transplantation. *J. Neurosci.* 19:7529–7536.

Kim, Y., and L.O. Trussell. 2007. Ion channels generating complex spikes in cartwheel cells of the dorsal cochlear nucleus. *J. Neurophysiol.* 97:1705–1725.

Komuro, H., and T. Kumada. 2005. $Ca^{2+}$ transients control CNS neuronal migration. *Cell Calcium.* 37:387–393.

Kononenko, N.I., L.R. Shao, and F.E. Dudek. 2004. Riluzole-sensitive slowly inactivating sodium current in rat suprachiasmatic nucleus neurons. *J. Neurophysiol.* 91:710–718.

Kriegstein, A.R., and S.C. Noctor. 2004. Patterns of neuronal migration in the embryonic cortex. *Trends Neurosci.* 27:392–399.

Levine, J.M., R. Reynolds, and J.W. Fawcett. 2001. The oligodendrocyte precursor cell in health and disease. *Trends Neurosci.* 24:39–47.

Levison, S.W., and J.E. Goldman. 1993. Both oligodendrocytes and astrocytes develop from progenitors in the subventricular zone of postnatal rat forebrain. *Neuron.* 10:201–212.

Lin, S.C., and D.E. Bergles. 2004a. Synaptic signaling between GABAergic interneurons and oligodendrocyte precursor cells in the hippocampus. *Nat. Neurosci.* 7:24–32.

Lin, S.C., and D.E. Bergles. 2004b. Synaptic signaling between neurons and glia. *Glia.* 47:290–298.

Liu, X., Q. Wang, T.F. Haydar, and A. Bordey. 2005. Nonsynaptic GABA signaling in postnatal subventricular zone controls proliferation of GFAP-expressing progenitors. *Nat. Neurosci.* 8:1179–1187.

Luskin, M.B., and K. McDermott. 1994. Divergent lineages for oligodendrocytes and astrocytes originating in the neonatal forebrain subventricular zone. *Glia.* 11:211–226.

Manent, J.B., and A. Represa. 2007. Neurotransmitters and brain maturation: early paracrine actions of GABA and glutamate modulate neuronal migration. *Neuroscientist.* 13:268–279.

Maric, D., Q.Y. Liu, I. Maric, S. Chaudry, Y.H. Chang, S.V. Smith, W. Sieghart, J.M. Fritschy, and J.L. Barker. 2001. GABA expression dominates neuronal lineage progression in the embryonic rat neocortex and facilitates neurite outgrowth via GABA(A) autoreceptor/$Cl^-$ channels. *J. Neurosci.* 21:2343–2360.

Marty, A., and I. Llano. 2005. Excitatory effects of GABA in established brain networks. *Trends Neurosci.* 28:284–289.

Menn, B., J.M. Garcia-Verdugo, C. Yaschine, O. Gonzalez-Perez, D. Rowitch, and A. Alvarez-Buylla. 2006. Origin of oligodendrocytes in the subventricular zone of the adult brain. *J. Neurosci.* 26:7907–7918.

Nguyen, L., J.M. Rigo, V. Rocher, S. Belachew, B. Malgrange, B. Rogister, P. Leprince, and G. Moonen. 2001. Neurotransmitters as early signals for central nervous system development. *Cell Tissue Res.* 305:187–202.

Nguyen, L., B. Malgrange, I. Breuskin, L. Bettendorff, G. Moonen, S. Belachew, and K.M. Rigo. 2003. Autocrine/paracrine activation of the GABA(A) receptor inhibits the proliferation of neurogenic polysialylated neural cell adhesion molecule-positive (PSA-NCAM+) precursor cells from postnatal striatum. *J. Neurosci.* 23:3278–3294.

Nishiyama, A., X.H. Lin, N. Giese, C.H. Heldin, and W.B. Stallcup. 1996. Co-localization of NG2 proteoglycan and PDGF alpha-receptor on O2A progenitor cells in the developing rat brain. *J. Neurosci. Res.* 43:299–314.

Nishiyama, A., M. Watanabe, Z. Yang, and J. Bu. 2002. Identity, distribution, and development of polydendrocytes: NG2-expressing glial cells. *J. Neurocytol.* 31:437–455.

Owens, D.F., and A.R. Kriegstein. 2002. Is there more to GABA than synaptic inhibition? *Nat. Rev. Neurosci.* 3:715–727.

Paukert, M., and D.E. Bergles. 2006. Synaptic communication between neurons and $NG2^+$ cells. *Curr. Opin. Neurobiol.* 16:515–521.

Platel, J.C., S. Boisseau, A. Dupuis, J. Brocard, A. Poupard, M. Savasta, M. Villaz, and M. Albrieux. 2005. $Na^+$ channel-mediated $Ca^{2+}$ entry leads to glutamate secretion in mouse neocortical preplate. *Proc. Natl. Acad. Sci. USA.* 102:19174–19179.

Ptak, K., G.G. Zummo, G.F. Alheid, T. Tkatch, D.J. Surmeier, and D.R. McCrimmon. 2005. Sodium currents in medullary neurons isolated from the pre-Bötzinger complex region. *J. Neurosci.* 25:5159–5170.

Represa, A., and Y. Ben-Ari. 2005. Trophic actions of GABA on neuronal development. *Trends Neurosci.* 28:278–283.

Rose, C.R., S.G. Waxman, and B.R. Ransom. 1998. Effects of glucose deprivation, chemical hypoxia, and simulated ischemia on $Na^+$ homeostasis in rat spinal cord astrocytes. *J. Neurosci.* 18:3554–3562.

Rosenberg, L.J., Y.D. Teng, and J.R. Wrathall. 1999. Effects of the sodium channel blocker tetrodotoxin on acute white matter pathology after experimental contusive spinal cord injury. *J. Neurosci.* 19:6122–6133.

Rush, A.M., S.D. Dib-Hajj, and S.G. Waxman. 2005. Electrophysiological properties of two axonal sodium channels, Nav1.2 and Nav1.6, expressed in mouse spinal sensory neurones. *J. Physiol.* 564:803–815.

Ryu, S., B. Liu, J. Yao, Q. Fu, and F. Qin. 2007. Uncoupling proton activation of vanilloid receptor TRPV1. *J. Neurosci.* 27:12797–12807.

Semyanov, A., M.C. Walker, D.M. Kullmann, and R.A. Silver. 2004. Tonically active GABA A receptors: modulating gain and maintaining the tone. *Trends Neurosci.* 27:262–269.

Sipilä, S.T., K. Huttu, I. Soltesz, J. Voipio, and K. Kaila. 2005. Depolarizing GABA acts on intrinsically bursting pyramidal neurons to drive giant depolarizing potentials in the immature hippocampus. *J. Neurosci.* 25:5280–5289.

Sipilä, S.T., K. Huttu, J. Voipio, and K. Kaila. 2006. Intrinsic bursting of immature CA3 pyramidal neurons and consequent giant depolarizing potentials are driven by a persistent $Na^+$ current and terminated by a slow $Ca^{2+}$ -activated $K^+$ current. *Eur. J. Neurosci.* 23:2330–2338.

Slodzinski, M.K., and M.P. Blaustein. 1998. $Na^+/Ca^{2+}$ exchange in neonatal rat heart cells: antisense inhibition and protein half-life. *Am. J. Physiol.* 275:C459–C467.

Small, R.K., P. Riddle, and M. Noble. 1987. Evidence for migration of oligodendrocyte-type-2 astrocyte progenitor cells into the developing rat optic nerve. *Nature.* 328:155–157.

Sontheimer, H., J. Trotter, M. Schachner, and H. Kettenmann. 1989. Channel expression correlates with differentiation stage during the development of oligodendrocytes from their precursor cells in culture. *Neuron.* 2:1135–1145.

Soria, J.M., and M. Valdeolmillos. 2002. Receptor-activated calcium signals in tangentiallly migrating cortical cells. *Cereb. Cortex.* 12:831–839.

Spassky, N., C. Goujet-Zalc, E. Parmantier, C. Olivier, S. Martinez, A. Ivanova, K. Ikenaka, W. Macklin, I. Cerruti, B. Zalc, and J.L. Thomas. 1998. Multiple restricted origin of oligodendrocytes. *J. Neurosci.* 18:8331–8343.

Stallcup, W.B. 2002. The NG2 proteoglycan: Past insights and future prospects. *J. Neurocytol.* 31:423–435.

Stys, P.K., S.G. Waxman, and B.R. Ransom. 1992. Ionic mechanisms of anoxic injury in mammalian CNS white matter: role of $Na^+$ channels and $Na^+$-$Ca^{2+}$ exchanger. *J. Neurosci.* 12:430–439.

Stys, P.K., H. Sontheimer, B.R. Ransom, and S.G. Waxman. 1993. Noninactivating, tetrodotoxin-sensitive $Na^+$ conductance in rat optic nerve axons. *Proc. Natl. Acad. Sci. USA.* 90:6976–6980.

Suzuki, S.O., and J.E. Goldman. 2003. Multiple cell populations in the early postnatal subventricular zone take distinct migratory pathways: A dynamic study of glial and neuronal progenitor migration. *J. Neurosci.* 23:4240–4250.

Thurneysen, T., D.A. Nicoll, K.D. Philipson, and H. Porzig. 2002. Sodium/calcium exchanger subtypes NCX1, NCX2 and NCX3 show cell-specific expression in rat hippocampus cultures. *Brain Res. Mol. Brain Res.* 107:145–156.

Vautrin, J., D. Maric, M. Sukhareva, A.E. Schaffner, and J.E. Barker. 2000. Surface-accessible GABA supports tonic and quantal synaptic transmission. *Synapse.* 37:38–55.

Waxman, S.G., M.J. Craner, and J.A. Black. 2004. $Na^+$ channel expression along axons in multiple sclerosis and its models. *Trends Pharmacol. Sci.* 25:584–591.

Wilson, M. 2004. Synaptic physiology: plenty of models to choose from. *Curr. Biol.* 14:R666–R667.

Wu, W., K. Wong, J. Chen, Z. Jiang, S. Dupuis, J.Y. Wu, and Y. Rao. 1999. Directional guidance of neuronal migration in the olfactory system by the protein Slit. *Nature.* 400:331–336.

Wu, Y., W. Wang, A. Díez-Sampedro, and G.B. Richerson. 2007. Nonvesicular inhibitory neurotransmission via reversal of the GABA transporter GAT-1. *Neuron.* 56:851–865.

Xu, X., and P. Shrager. 2005. Dependence of axon initial segment formation on $Na^+$ channel expression. *J. Neurosci. Res.* 79:428–441.

Yamada, J., A. Okabe, H. Toyoda, W. Kilb, H.J. Luhmann, and A. Fukuda. 2004. $Cl^-$ uptake promoting depolarizing GABA actions in immature rat neocortical neurones is mediated by NKCC1. *J. Physiol.* 557:829–841.

Zeng, J., R.K. Powers, G. Newkirk, M. Yonkers, and M.D. Binder. 2005. Contribution of persistent sodium currents to spike-frequency adaptation in rat hypoglossal motoneurons. *J. Neurophysiol.* 93:1035–1041.

Zerlin, M., S.W. Levison, and J.E. Goldman. 1995. Early patterns of migration, morphogenesis, and intermediate filament expression of subventricular zone cells in the postnatal rat forebrain. *J. Neurosci.* 15:7238–7249.

Zhang, H., L. Vutskits, V. Calaora, P. Durbec, and J.Z. Kiss. 2004. A role for the polysialic acid-neural cell adhesion molecule in PDGF-induced chemotaxis of oligodendrocyte precursor cells. *J. Cell Sci.* 117:93–103.

Zhang, J.M., H.K. Wang, C.Q. Ye, W. Ge, Y. Chen, Z.L. Jiang, C.P. Wu, M.M. Poo, and S. Duan. 2003. ATP released by astrocytes mediates glutamatergic activity-dependent heterosynaptic suppression. *Neuron.* 40:971–982.

Zhang, L.L., H.R. Pathak, D.A. Coulter, M.A. Freed, and N. Vardi. 2006. Shift of intracellular chloride concentration in ganglion and amacrine cells of developing mouse retina. *J. Neurophysiol.* 95:2404–2416.

Zhang, Z., G. Chen, W. Zhou, A. Song, W. Wang, T. Xu, Q.M. Luo, X.S. Gu, and S. Duan. 2007. Regulated ATP release from astrocytes via lysosome exocytosis. *Nat. Cell Biol.* 9:945–953.

Zheng, J.Q., and M.M. Poo. 2007. Calcium signaling in neuronal motility. *Annu. Rev. Cell Dev. Biol.* 23:375–404.

Zheng, J.Q., M. Felder, J.A. Connor, and M.M. Poo. 1994. Turning of nerve growth cones induced by neurotransmitters. *Nature.* 368:140–144.

Ziskin, J.L., A. Nishiyama, M. Rubio, M. Fukaya, and D.E. Bergles. 2007. Vesicular release of glutamate from unmyelinated axons in white matter. *Nat. Neurosci.* 10:321–330.